Cell Reports

Resource

Circadian rhythm heterogeneity modulates drug response variations in neuroblastoma models

Graphical abstract

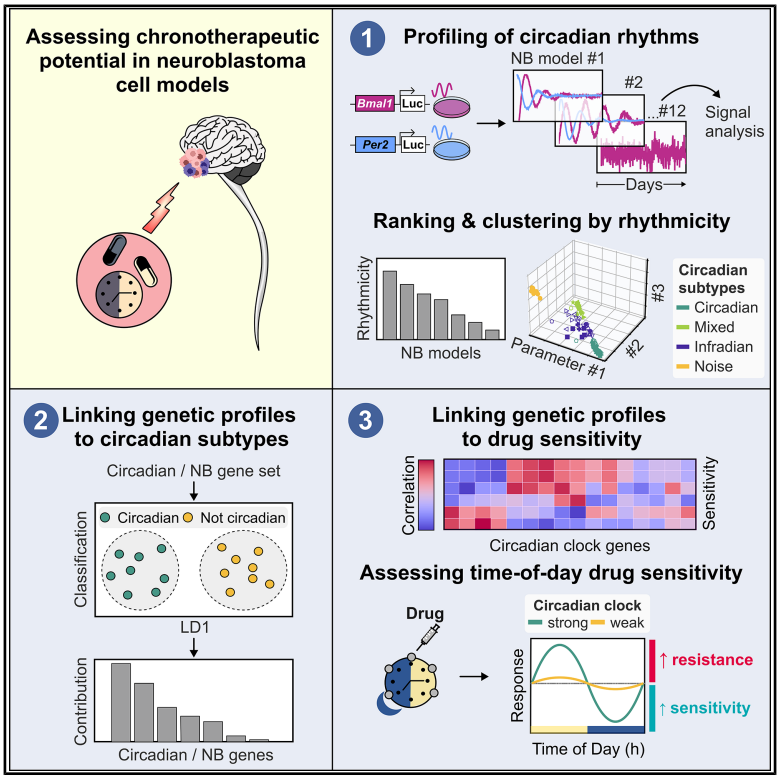

Highlights

- Long-term live-cell imaging reveals circadian oscillations in neuroblastoma cells
- Deep circadian phenotyping shows diverse clock dynamics in neuroblastoma cell models
- Genetic profiles associate with circadian rhythm strength and drug sensitivity patterns
- Circadian-competent neuroblastoma cells vary in drug sensitivity by time of day

Authors

Carolin Ector, Christoph Schmal, Jeff Didier, ..., Achim Kramer, Hanspeter Herzel, Adrián E. Granada

Correspondence

adrian@granadalab.org

In brief

Ector et al. uncover circadian heterogeneity across neuroblastoma cell models and link rhythmic strength to drug sensitivity. Their findings suggest that circadian competence may influence treatment outcomes, pointing to chronotherapy as a potential avenue for improving pediatric cancer care.

Ector et al., 2026, Cell Reports *45*, 116975
February 24, 2026
https://doi.org/10.1016/j.celrep.2026.116975

CellPress

Cell Reports

CellPress
OPEN ACCESS

Resource

Circadian rhythm heterogeneity modulates drug response variations in neuroblastoma models

Carolin Ector,[1,2,9] Christoph Schmal,[2] Jeff Didier,[3] Sébastien De Landtsheer,[3] Johannes H. Schulte,[4,10] Ulrich Keilholz,[1,5] Thomas Sauter,[3] Achim Kramer,[7] Hanspeter Herzel,[2,6] and Adrián E. Granada[8,11,*]

[1]Charité Comprehensive Cancer Center, Charité – Universitätsmedizin Berlin, 10117 Berlin, Germany
[2]Institute for Theoretical Biology, Humboldt-Universität zu Berlin, 10115 Berlin, Germany
[3]Department of Life Sciences and Medicine, University of Luxembourg, 4365 Esch-sur-Alzette, Luxembourg
[4]Department of Pediatric Oncology, Hematology and Stem Cell Transplantation, Charité – Universitätsmedizin Berlin, Charitéplatz 1, 10117 Berlin, Germany
[5]German Cancer Consortium (DKTK), Berlin, Germany
[6]Charité – Universitätsmedizin Berlin, 10117 Berlin, Germany
[7]Laboratory of Chronobiology, Charité – Universitätsmedizin Berlin, 10117 Berlin, Germany
[8]Work Conducted While Affiliated with Charité – Universitätsmedizin Berlin, 10117 Berlin, Germany
[9]Present address: The Francis Crick Institute, London NW1 1AT, UK
[10]Present address: Clinic for Pediatrics and Adolescent Medicine, Universitätsklinikum Tübingen, Hoppe-Seyler-Str. 1, 72076 Tübingen, Germany
[11]Lead contact
*Correspondence: adrian@granadalab.org
https://doi.org/10.1016/j.celrep.2026.116975

SUMMARY

Circadian clocks regulate essential cellular functions and influence cancer development and treatment outcomes. Aligning therapy with circadian rhythms can improve efficacy and reduce toxicity, yet whether neuroblastoma, a heterogeneous pediatric tumor, maintains circadian function remains unclear. Here, we systematically profiled circadian dynamics across 12 neuroblastoma cell models using long-term bioluminescence assays and computational analysis. Our findings reveal heterogeneous circadian patterns ranging from robust to arrhythmic, which we linked to distinct neuroblastoma genetic features. By integrating drug sensitivity data, we identified candidate compounds whose effectiveness correlates with circadian expression profiles. Moreover, time-of-day treatment assays with the ALK inhibitor lorlatinib and frontline chemotherapeutics revealed distinct temporal drug responses that were more pronounced in circadian-competent than weakly rhythmic cell lines. Together, these findings establish circadian heterogeneity as a previously unrecognized dimension of neuroblastoma biology and highlight the therapeutic potential of chronotherapy approaches for improved treatment efficacy.

INTRODUCTION

Circadian clocks are inheritable timekeepers that have evolved among diverse life forms in response to daily fluctuations in light and temperature.[1,2] In mammals, a master pacemaker located in the suprachiasmatic nucleus (SCN) of the hypothalamus coordinates the overall rhythm of the organism, while peripheral tissue clocks maintain their own intrinsic oscillations.[3,4] Hence, circadian rhythms can be detected from the level of the entire organism down to individual cells, underscoring their fundamental biological importance.[3]

At the cellular level, the generation of intracellular rhythms relies on interconnected transcriptional-translational feedback loops (TTFLs).[5] Central to this process are heterodimers formed by BMAL1 and CLOCK, which bind to E-box elements in the promoters of *Period* (*Per*) and *Cryptochrome* (*Cry*) genes, thereby promoting their transcription. In turn, PER and CRY proteins inhibit the activity of the BMAL1-CLOCK heterodimers, effectively closing the negative feedback loop. Complementary feedback loops, involving genes such as *Reverb*, *Ror*, and *Dbp*, further adjust the period, amplitude, and phase of circadian oscillations, contributing to the system's flexibility and resilience.[6]

Circadian rhythms regulate approximately 40% of protein-coding genes,[7] orchestrating crucial physiological processes such as cell cycle progression,[8] metabolism,[9] and DNA repair.[10] This widespread influence underscores the clock's integral role in maintaining cellular homeostasis and its impact on various pathophysiological conditions.[11] While the disruption of circadian rhythms has been implicated with diverse cancer types,[12] a growing body of research shows that rhythmicity can persist in cancer cells to varying degrees.[13–17] In cancer therapy, circadian rhythms can be effectively leveraged to time treatments with the patient's natural biological cycles, potentially enhancing drug efficacy and reducing side effects, a treatment concept referred to as chronotherapy.[18] Despite these promising insights, the circadian clock status remains poorly understood in

many cancers, including neuroblastoma (NB), the most prevalent cancer in infancy, accounting for over 10% of childhood cancer-related deaths.[19] This pediatric tumor arises from fetal neural crest cells and is marked by considerable biological and clinical heterogeneity. Approximately 50% of patients are classified as high risk, with 5-year survival rates falling below 40%.[20] The aggressiveness of the disease is closely linked to a range of genetic alterations, including the amplification of the proto-oncogene MYCN, rearrangements at the TERT locus, inactivating mutations in ATRX and the activation of ALK.[21]

To investigate circadian properties in neuroblastoma, we conducted deep circadian phenotyping[13,22] across 12 distinct NB cell models. We combined long-term high-resolution bioluminescence assays of core clock genes with an in-depth computational characterization of the circadian signals, which revealed widespread but heterogeneous circadian oscillations. Integrating gene expression data, we identified circadian and NB-specific signatures distinguishing strongly rhythmic from weakly rhythmic models. Analysis of public drug sensitivity datasets uncovered compounds whose efficacy correlated with circadian gene activity, and complementary time-of-day assays with lorlatinib, cisplatin, and doxorubicin revealed distinct time-of-day sensitivity that was more pronounced in circadian-competent lines. Together, this systematic profiling establishes a resource linking circadian heterogeneity to genetic background and drug response, providing a foundation for circadian-aligned therapies in neuroblastoma.

RESULTS

Circadian phenotypes in neuroblastoma cell models

To record circadian signals in a wide range of neuroblastoma cell lines, we engineered them to stably express luciferase (Luc) reporters of two key circadian clock genes, *Bmal1* and *Per2*. We then generated high-resolution 5-day bioluminescence recordings of the reporter cell lines (Figure 1A), revealing considerable variability among them (Figure 1B and S1A, B; see Table S1 for clinical features of the cell models). For instance, while SKNSH showed robust oscillations for 5 days, GIMEN exhibited clear but rapidly damping rhythms, SH-SY5Y oscillated with extended periods, while CHP212 did not display detectable rhythmicity (Figure 1B). Interestingly, the *Bmal1* and *Per2* signals in GIMEN cells were nearly anti-phasic, indicative of a functional circadian clock network, whereas in SKNSH cells they displayed a pronounced phase shift.

To better characterize circadian rhythmicity, we applied discrete wavelet-based multiresolution analysis (MRA; see STAR Methods), decomposing detrended signals into noise (1–4 h), ultradian (4–16 h), circadian (16–32 h), and infradian (32–256 h) components. This revealed that 76.8% of the GIMEN-*Bmal1* signal lies within the circadian range, with minimal contribution of noise (0.3%; Figure 1C). However, an appreciable 18.8% of the signal resided in the infradian band, suggesting the presence of additional oscillatory dynamics. Extracting the circadian component across various NB models enabled us to rank them by rhythmic strength. Instead of a binary division into rhythmic or arrhythmic, the analysis revealed a continuum of rhythmicity (Figure 1D), consistent with our earlier findings in breast cancer models.[13]

Given the diverse clinical backgrounds of the patients from whom each NB cell line was derived (Table S1), we performed an exploratory analysis to investigate whether circadian components retained any association with basic clinical features such as patient age, biological sex, or ALK mutation status. Stratification by clinical features suggested an association whereby cell lines from patients older than two years tended to exhibit stronger circadian components (Figure S2A). Furthermore, female-derived and ALK-mutated samples tended toward higher rhythmicity compared to male-derived and ALK wild-type samples, respectively (Figures S2B and S2C). These trends are consistent with reported age- and sex-dependent variation in circadian regulation in humans.[23,24] However, given the limited sample size and the multiple biological differences of established cell lines from primary tumors, these associations should be interpreted with caution. We therefore focused subsequent analyses on mechanistic links within the cell lines themselves.

Next, we explored the presence of circadian phenotypes in neuroblastoma by conducting a principal component analysis (PCA) on the four coarse-grained MRA frequency components: noise, ultradian, circadian, and infradian. PCA revealed four distinct clusters, consistent across combined *Bmal1*/*Per2* data (Figure 1E) and reporter-separate analyses (Figures S3A and S3B), which supports the presence of intrinsic circadian subtypes. Loadings indicated that all but the ultradian component contributed substantially to variance (Figures S3C and S3D). To refine this classification, we therefore applied *k*-means clustering ($k = 4$) on noise, circadian, and infradian components. This analysis assigned each sample to a cluster defined by predominant variance in either of these patterns or a mixed pattern that fell between the circadian and infradian ranges (Figures 1F, 1G, S3E, and S3F; see Table S2 for detailed results).

In summary, our integrative framework revealed that samples from three specific models (SKNSH, NGP, and GIMEN) consistently fell within the circadian cluster, affirming the existence of stable circadian phenotypes. In contrast, most of the cell lines exhibited patterns that were either mixed circadian or infradian, with two models only (SH-SY5Y and CHP212) showing a complete absence of circadian rhythmicity. This highlights the diverse and complex nature of the circadian clock within neuroblastoma cell lines.

Circadian signal stability and variability in neuroblastoma

Building on the observed circadian phenotypes, we next characterized signal parameters using two complementary approaches: harmonic regression, fitting a stochastic damped oscillator to each detrended trace to capture time-averaged properties, and continuous wavelet transform (CWT) to reveal time-dependent changes in non-stationary signals.[25] Importantly, we focused our analyses on recordings that classified as circadian or mixed circadian (Figure 1G).

Harmonic regression of detrended signal traces (Figure 2A) revealed predominantly prolonged signal periods of up to 36 h (Figure 2B). Only NGP-, SKNAS-, and GIMEN-*Bmal1* cells exhibited periods close to a 24-h cycle (Figure 2B). All cell lines showed damped oscillations (Figure S1), though the degree varied: LAN5 and SKNAS decayed within one cycle, whereas most

CellPress
OPEN ACCESS

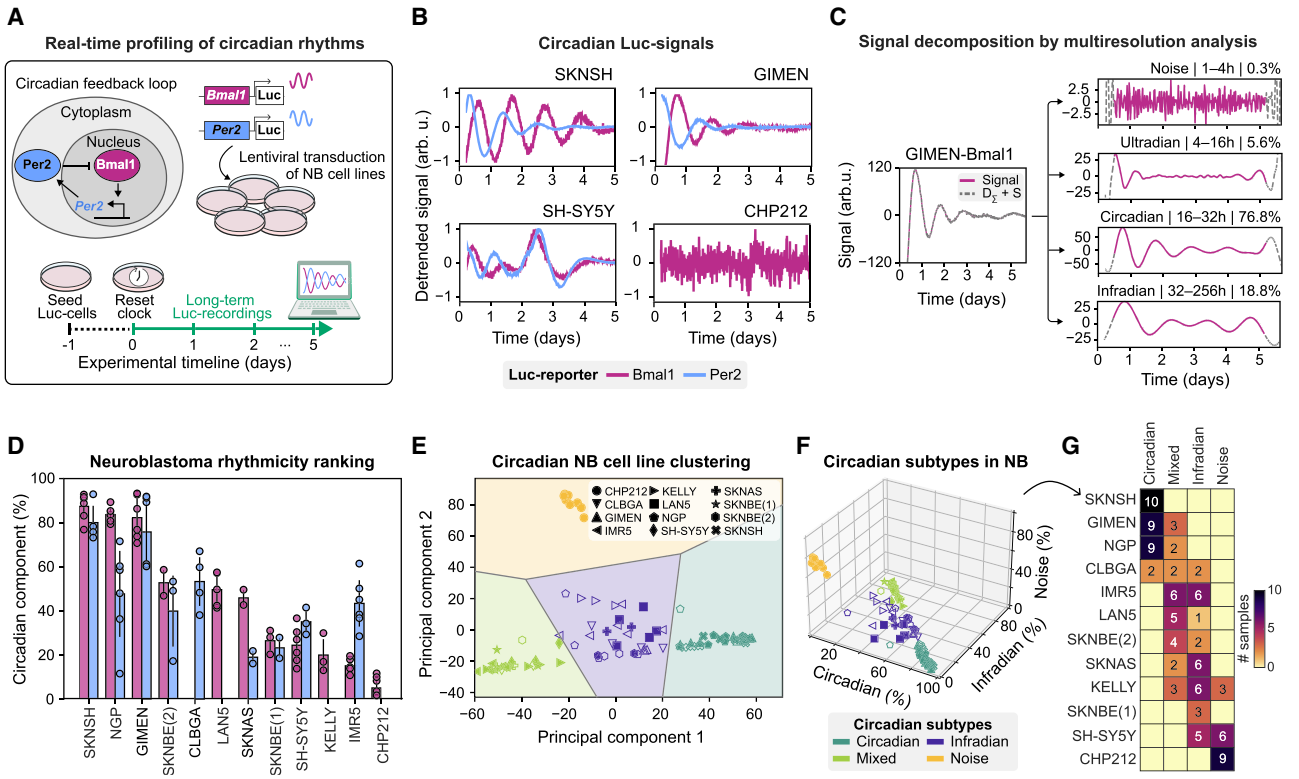

Figure 1. Real-time profiling of circadian rhythms in neuroblastoma cell lines

(A) Schematic of the experimental strategy to monitor circadian rhythms in neuroblastoma (NB) cell lines. NB cell lines stably expressing luciferase (Luc) reporters for *Bmal1* and *Per2* were generated via lentiviral transduction, enabling real-time expression monitoring. Following a circadian clock reset, Luc signal from cell populations was recorded over multiple days.

(B) Overlay of detrended *Bmal1* and *Per2* signal traces (color-coded) of four NB cell lines.

(C) Multiresolution analysis (MRA) of detrended GIMEN-*Bmal1* signal, breaking it down into four frequency components, with each component's percentage representing its share of the total signal.

(D) Bar plot ranking cell lines by their MRA circadian component, grouped and color-coded for *Bmal1*- and *Per2* signals. Data represent the mean ± SD across individual samples (see exact numbers below).

(E) Principal component analysis (PCA) biplot showing the distribution of all *Bmal1*- and *Per2*-Luc samples ($n = 106$) along the first two PCs, calculated from the four MRA frequency components. Cell models are distinguished by markers. PCA clusters are outlined and color-coded for clarity.

(F) 3D scatterplot depicting the distribution of all *Bmal1*- and *Per2*-Luc samples ($n = 106$) along the MRA circadian, infradian, and noise axes. Clusters, determined by the dominant signal components, are color-coded for clarity.

(G) Heatmap showing the number of samples for each cell line (row) per circadian cluster (columns), corresponding to (F).

Data shown in (D)–(G) are derived from two biological replicates and technical triplicates ($n = 6$ samples per Luc reporter). NGP-*Bmal1* and SH-SY5Y-*Per2* were assayed in technical duplicates in one experiment ($n = 5$). CHP212-*Bmal1* was assayed in three biological replicates and technical triplicates ($n = 9$). SKNSH-*Per2* was assayed in a single sample in one experiment ($n = 4$). SKNAS-*Per2* was assayed in a single experiment in technical duplicates ($n = 2$). SKNBE(1) and SKNBE(2) samples were assayed in a single experiment in technical triplicates ($n = 3$).

retained half their amplitude beyond the first oscillation (Figure 2C). Interestingly, period length and damping were correlated, with slower decay linked to longer periods ($R^2 = 0.48$, Spearman $r = -0.77$, $p = 0.021$). These coupled signatures of amplitude loss and period prolongation suggest rapid desynchronization and weak extracellular coupling, processes that may promote tumor growth.[26,27]

To assess how circadian features change over time, we next applied CWT, which generates a time-period power spectrum, thereby illustrating the range and relative power of oscillatory components within a specific period range (Figure 2E). Tracking the main oscillatory component ("ridge") revealed time-dependent variation in period and amplitude. In GIMEN-*Bmal1* cells, rhythms remained stable for ~3.5 days before decaying and lengthening to ~30 h (Figure 2F), indicative of a loss of population synchrony. By quantifying the ridge length as a proxy for circadian clock strength, with longer, continuous ridges indicating robust signals, we observed a gradual ranking across models, where SKNSH displayed the longest ridge (Figure 2G). This finding aligns with its high ranking in the circadian component analysis and its clustering outcomes (see Figures 1D–1G).

We next aggregated continuous periods across replicates to assess potential variability (Figure 2H). Consistent with the stationary analysis (Figure 2B), periods ranged from short to extended, with circadian-clustered models closest to 24 h. LAN5, despite short periods in harmonic regression, averaged

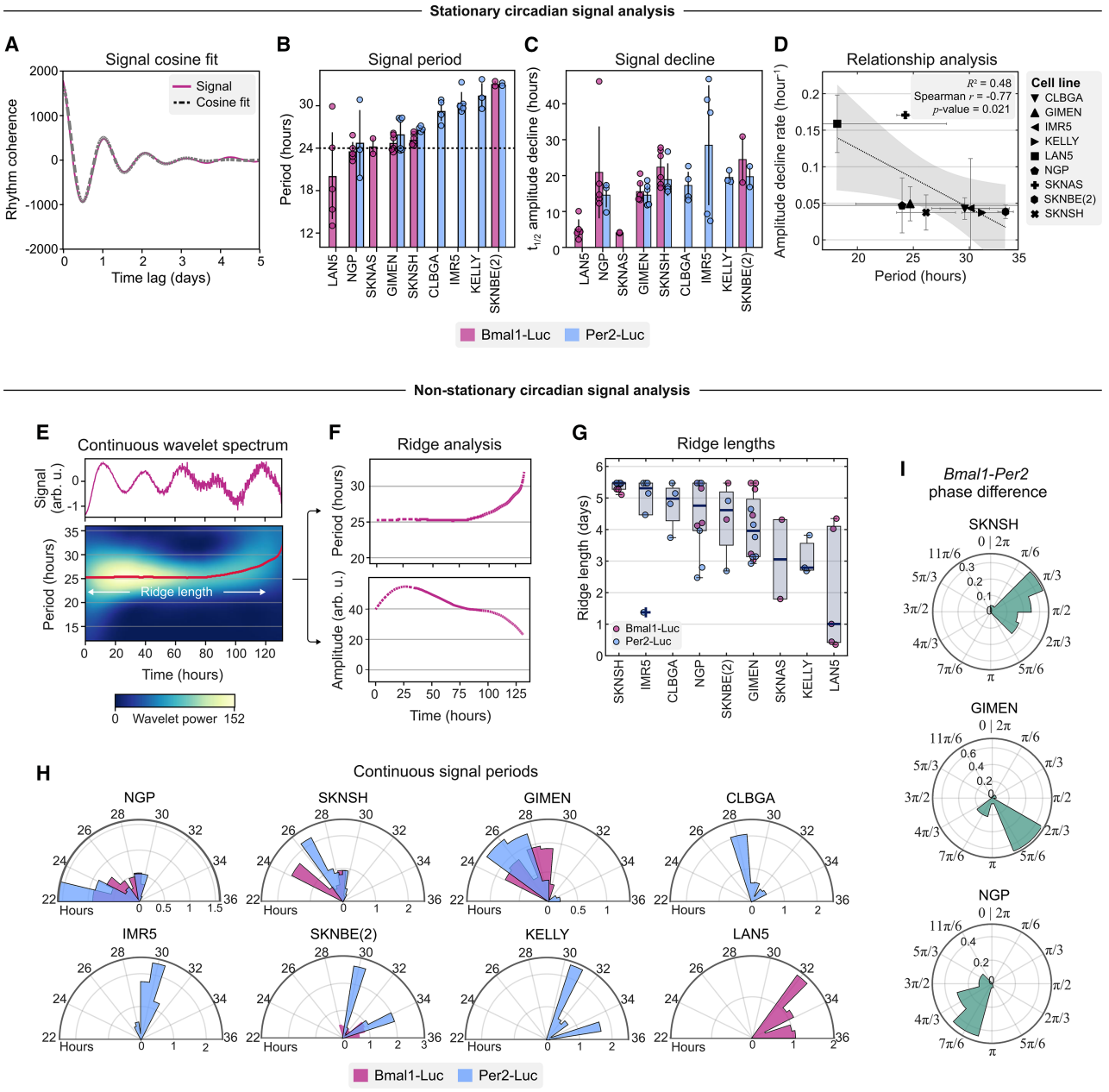

Figure 2. Deep circadian phenotyping across neuroblastoma cell line models

(A) Non-linear least squares fitting (dashed gray curve) to GIMEN-*Bmal1*-Luc signal (pink curve).

(B) Bar plot of NB cell lines ranked by mean signal periods, determined via non-linear least squares fitting and color-coded for *Bmal1*- or *Per2* signals. Data represent the mean ± SD across individual samples. Dashed line = 24 h. Note that one NGP-*Per2* sample (period = 41.1 h) is cut from the axis but contributed to the mean ± SD.

(C) See (B) but shown for mean amplitude decline half-life ($t_{1/2}$). The order follows the same scheme as in (B).

(D) Relationship between amplitude decay rates and circadian periods across NB cell lines (n = 7, distinguished by markers), as determined by nonlinear least squares fitting. The gray area denotes the 95% confidence interval, with model accuracy shown by R^2 values. Spearman's correlation coefficient (r) and its p value are noted in the legend. Data represents the mean ± SD across individual samples across Luc-reporters. Sample sizes in (B)–(D) per available reporter are LAN5, NGP-*Bmal1*, and IMR5 (n = 5); SKNAS and SKNBE(2) (n = 2); GIMEN and SKNSH-*Bmal1* (n = 6); NGP-*Per2*, SKNSH-*Per2*, and CLBGA (n = 4); and KELLY (n = 3).

(E) Continuous wavelet transform (CWT) on detrended and normalized GIMEN-*Bmal1* signal (top). The corresponding wavelet spectrum (bottom) displays time-resolved periods, with the primary oscillatory component (*ridge*) highlighted in red.

(F) Ridge readout of continuous periods (top) and amplitudes (bottom), corresponding to the CWT analysis in (E).

(G) Boxplot displaying CWT ridge lengths from *Bmal1*-/*Per2* signals across cell lines. The box edges indicate the 25th and 75th percentiles, with whiskers extending to values within 1.5 times the interquartile range. The median is shown as a dark blue horizontal line.

(legend continued on next page)

~34 h here, likely due to excluding traces with ridges too short to track, underscoring the value of time-resolved analysis. Building on the insights into temporal dynamics of both period and signal stability, we further assessed the *Bmal1-Per2* phase differences over time for the three most circadian NB cell models: SKNSH, GIMEN, and NGP. Despite their overall circadian behavior, their phase relationships diverged: SKNSH showed a ~4 h lag ($\pi/3$), GIMEN ~8–9 h, and NGP ~14 h (Figure 2I). Notably, the ~8 h lag resembles that reported for U2OS and MCF10A cells,[13] two highly circadian cell models,[14,15] suggesting that similar circadian clock timings may extend across different cell types.

To explore how circadian parameters relate to functional outputs, we further characterized the growth dynamics of the neuroblastoma cell line panel by long-term live-cell imaging (see STAR Methods). We first parametrized the normalized confluence data with a logistic function to obtain cell line-specific growth rates (Figure S4A). Next, we examined these growth rates in relation to circadian parameters derived from our deep phenotyping analysis (Figure S4B).

This revealed two significant associations: a negative correlation with the circadian component (R^2 = 0.57, r = −0.75, p = 0.012; Figure S4C) and a positive correlation with the circadian period (R^2 = 0.27, r = 0.52, p = 0.152; Figure S4D). These findings suggest that faster proliferating models display disrupted circadian rhythms, characterized by either weaker rhythms or prolonged periods.

In summary, our analysis reveals heterogeneous circadian properties in neuroblastoma cell models, with most cell lines exhibiting prolonged periods, variable damping and distinct *Bmal1-Per2* phase relationships. Time-resolved analyses revealed differences in signal stability that enabled ranking of circadian robustness. Importantly, weaker or lengthened rhythms link with faster cellular proliferation, suggesting that circadian impairment is functionally connected to tumor growth.

Linking circadian phenotypes to gene expression

Building upon the circadian phenotyping results, we next sought to understand how the rhythmic patterns of the NB cell lines relate to gene expression profiles by analyzing their molecular profiles from the Cancer Cell Line Encyclopedia (CCLE) DepMap 2022-Q2 (https://sites.broadinstitute.org/ccle/datasets).[28] Using both circadian and NB-specific genes, we classified cell models by their circadian component defined from deep circadian phenotyping. We first tested all circadian or NB-specific genes, then iteratively examined gene combinations to identify optimal predictive sets (Figure 3A). Core clock genes were defined as those essential for TTFL regulation whose disruption impairs rhythmicity,[5,29] while NB-specific genes were those commonly mutated or dysregulated in neuroblastoma.[30,31]

Cluster analysis of raw expression values for the circadian genes classified eight NB cell models, whose gene expression data were available, into two overarching clusters (Figure S5A). However, each cluster contained cell models with both high and low circadian oscillation components. Linear discriminant analysis (LDA) confirmed the poor predictive power of the full gene set, achieving only 25% accuracy by leave-one-out cross-validation (LOOCV) (Figures 3B and S5B). We therefore hypothesized that the circadian phenotype of each cell model might be more accurately predicted by a specific combination of genes. To test this, we systematically screened all possible gene combinations, from single genes up to sets of 15, and evaluated their classification performance. Both separation metrics, the ratio of between-class distance (BCD) to within-class distance (WCD; see Figure 3A), and LOOCV accuracy revealed a similar trend: the predictive power increased with the number of genes up to about 5–6, after which performance declined (Figures 3C and S5C). Notably, only combinations of 3–5 circadian genes consistently achieved high accuracy and well separation in the LDA space, indicating that small but specific subsets of circadian genes are sufficient to capture the circadian phenotype (Figures 3D, S5B, and S5D). Here, *Bmal1*, *Clock*, and *Rev-erbα* consistently appeared among the top-ranking genes.

Parallel analysis of NB-specific genes showed that while the full 11-gene panel separated models better than circadian genes (Figure 3E), it achieved 0% prediction accuracy (Figure S5E). Testing all 2,047 subsets revealed peak performance with 3–5 genes, after which accuracy declined (Figure 3F). These small subsets consistently reached 100% accuracy (Figures S5E and S5F), with *Phox2b* and *Ntrk2* emerging as most informative genes, frequently accompanied by *Atrx* (Figures 3G and S5G). Thus, as with circadian genes, a smaller number of NB-specific genes proved sufficient to classify circadian phenotypes.

These findings reveal that both circadian and NB-specific genes can be used to classify circadian phenotypes in the panel of neuroblastoma cell models, suggesting a potential interaction between oncogenic neuroblastoma pathways and circadian regulation.

Circadian gene expression and treatment timing shape drug responses in neuroblastoma cell models

Having linked circadian phenotypes to gene expression, we next examined how circadian regulators relate to drug sensitivity. Here, circadian regulators may influence cellular processes underlying drug response, potentially serving as biomarkers for therapeutic efficacy.

Using CCLE data from NB models with matched availability on expression and drug sensitivity data, linear regression and Spearman analysis revealed multiple correlations between circadian genes and drug activity (ActArea; Figure 4A; refer to Table S3 for the drugs' clinical relevance in NB). Negative regulators such as *Cry2* and *Per2* tended to anticorrelate with drug sensitivity, while positive regulators such as *Clock* and *Npas2* showed positive correlations (Figures 4A and 4B), suggesting that core network relationships are preserved. After Bonferroni correction, four associations remained significant: *Per2*-topotecan, *Rev-erbα*-paclitaxel, *Clock*-PF2341066, and *Rorγ*-PLX4720 (Figures 4A and 4C). Analyses of IC_{50} and EC_{50} data identified

(H) Probability-normalized, cell line-specific polar histograms of continuous signal periods for each Luc reporter (color-coded). Sample sizes in (G) and (H) are as described for (B)–(D), except for IMR5 (n = 6).
(I) Probability-normalized polar histograms of *Bmal1-Per2* phase differences for the specified cell lines, averaged over multiple combinations: SKNSH (n = 25), GIMEN (n = 36), and NGP (n = 26).

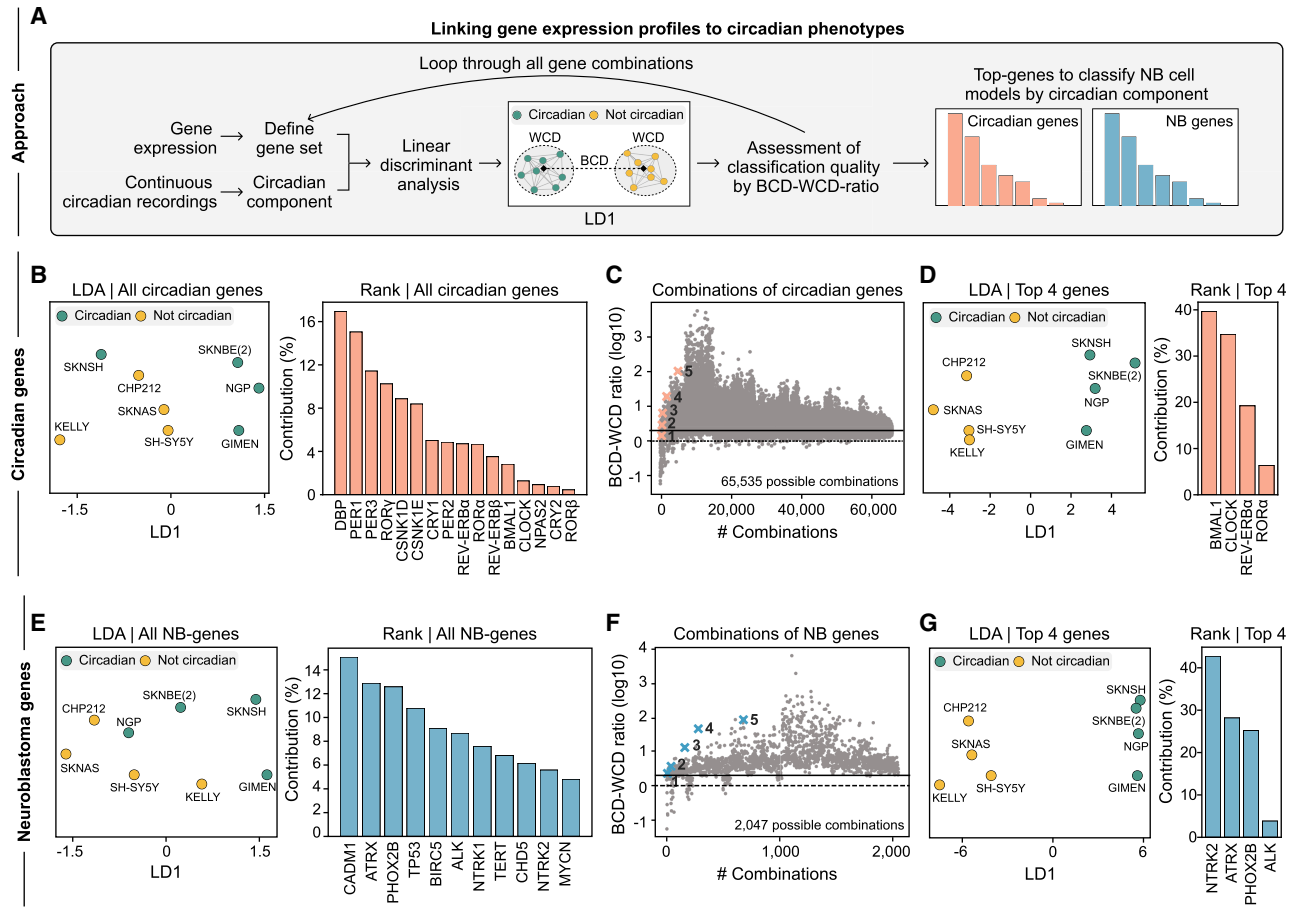

Figure 3. Linking gene expression levels to circadian phenotypes in neuroblastoma

(A) Overview of the linear discriminant analysis (LDA)-based approach used to investigate how circadian or neuroblastoma (NB)-specific genes influence circadian phenotypes across NB cell models. Each gene list was tested in various combinations to identify the subset of genes that most accurately predict circadian phenotypes. NB cell models were initially classified based on their characterized circadian component, determined through deep circadian phenotyping.

(B) *Left panel*: LDA on median-binarized circadian components (determined via MRA), using all 16 circadian genes as predictors. Cell models with circadian component values below or above the median are shown in yellow and green, respectively. The *x* axis represents the first linear discriminant (LD1), reflecting the greatest variance between these two groups. *Right panel*: bar plot ranking the 16 circadian genes by their individual contribution to the discriminative power of the LDA model.

(C) All possible combinations of circadian genes plotted against their corresponding log10 ratio of between-cluster distance (BCD) to within-cluster distance (WCD), an LDA-based metric of separation quality. The best-performing combinations up to five genes are marked with an X.

(D) See (B), here shown for LDA using the top 4 performing circadian genes as predictors.

(E) See (B), here shown for LDA using all 11 NB-specific genes.

(F) See (C), here shown for NB-specific genes.

(G) See (B), here shown for LDA using the top 4 performing NB-specific genes as predictors.

additional links, including *Dbp*-topotecan, *Per1*-TAE684, and *Clock*-panobinostat (Figures S6A and S6B). Together, these results highlight topotecan and ALK inhibitors as consistently associated with circadian gene expression, though effect direction varied by sensitivity metric. This shows that, despite the small sample sizes, topotecan consistently shows significant correlations with specific clock genes, while the direction of these associations (positive or negative) depends on the drug sensitivity metric employed.

We next sought to directly test whether neuroblastoma cell models exhibit time-of-day (ToD)-dependent drug responses. To do so, we performed ToD sensitivity assays using our established *in vitro* pipeline,[22] selecting five neuroblastoma cell lines from different ranges of the circadian rhythmicity spectrum: GIMEN and SKNSH (strong rhythmicity), SKNBE(2) (intermediate), and SH-SY5Y and CHP212 (weak rhythmicity). Following an established resetting-treatment protocol,[22] cells were treated at six circadian timepoints with three clinically relevant drugs: lorlatinib (ALK inhibitor), cisplatin (DNA crosslinker), and doxorubicin (DNA synthesis inhibitor; Figure 4D). GIMEN cells showed pronounced and consistent ToD-dependent responses across all tested drugs (Figure 4E, *left*), with lorlatinib eliciting the highest

CellPress
OPEN ACCESS

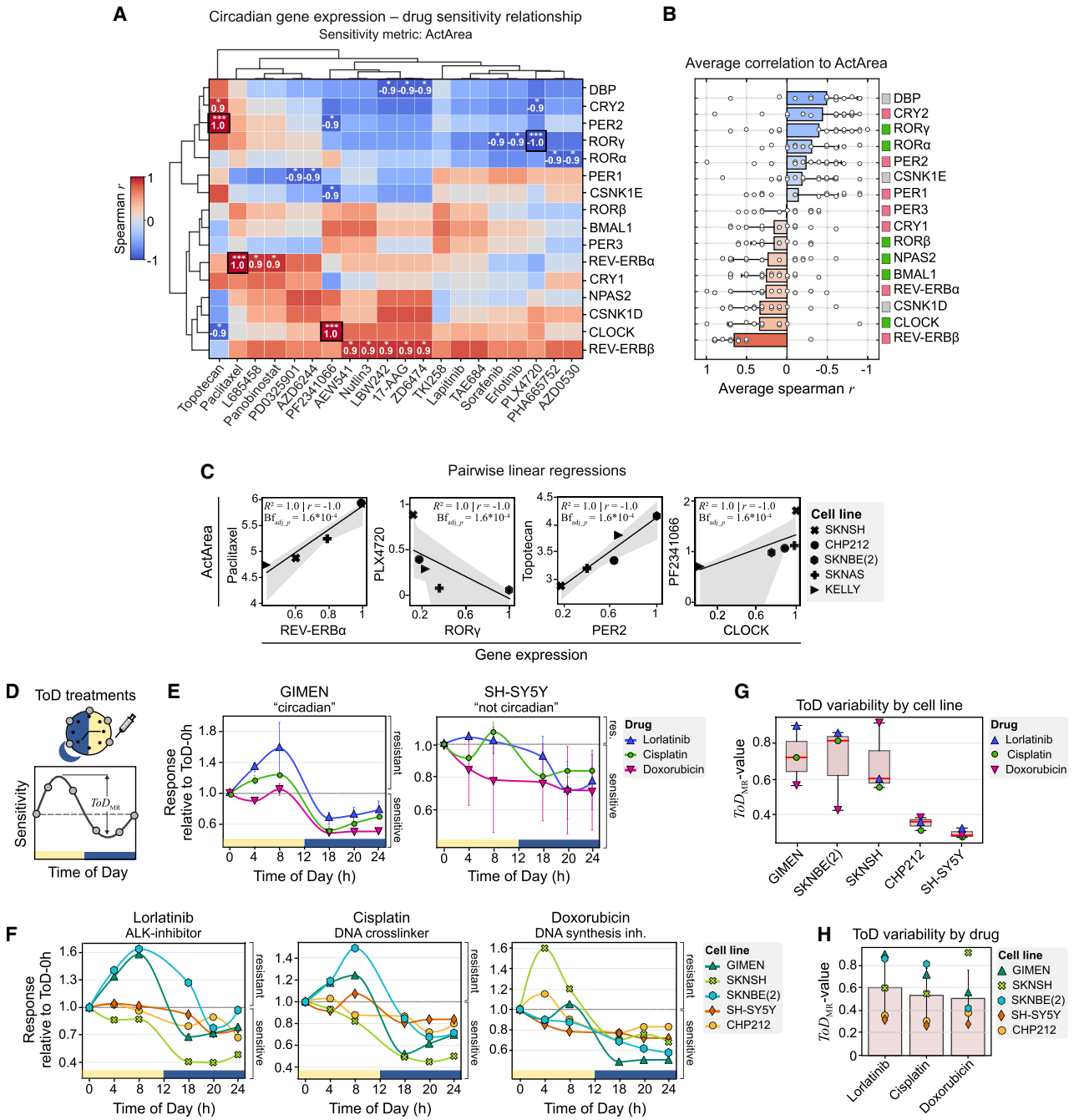

Figure 4. Correlation analysis of drug sensitivity and circadian gene expression in neuroblastoma cell lines

(A) Cluster map of Spearman correlation coefficients between ActArea values for multiple drugs and circadian gene expression across 6 NB cell lines, based on CCLE data. Significant correlations (two-sided *t* test with no adjustments made) are indicated by stars (* $p = 0.037$, *** $p = 1.4 \times 10^{-24}$). Correlations remaining significant after Bonferroni correction ($Bf_{adj\_p} = 1.6 \times 10^{-4}$) are outlined in black.

(B) Bar diagrams of average Spearman correlations between ActArea values ($n = 20$ drugs) and circadian gene expression, ranked by circadian genes in ascending order. Bars represent the mean ± SD, with individual ActArea-gene correlations overlaid as white circles. Only one-sided error bars are shown for clarity. Bar colors match the heatmap in (A). Gene colors: green = positive regulators; red = negative regulators; gray = stabilizing/modulating/output genes of the circadian clock network.

(C) Linear regression of Bonferroni-significant ActArea-gene pairs, with the shaded area representing the 95% confidence interval. R^2 values indicate model fit ($n = 6$ cell models).

(D) Schematic of time-of-day (ToD) drug treatments and resulting variability in responses across the day. Arrows indicate the maximum ToD response range (ToD_{MR}).

(legend continued on next page)

range in ToD responses between the most and least sensitive timepoints (ToD_{MR}) (2.3-fold differences). By contrast, weakly rhythmic SH-SY5Y cells exhibited only minimal and inconsistent ToD variation across all three drugs (Figure 4E, *right*).

When we examined ToD responses across all cell models, each drug generated distinct temporal dynamics (Figures 4F and S6C). While sensitivity generally increased at later circadian times, the magnitude and pattern of modulation varied considerably between drugs and cell lines. This heterogeneity became further apparent when ranking models by their average ToD_{MR} value, which revealed a clear stratification where circadian-competent lines consistently showed higher temporal modulation compared to weakly rhythmic models (Figure 4G). Supporting this pattern, the weakly rhythmic cell lines CHP212 and SH-SY5Y also exhibited greater inter-experimental variability, indicating less reproducible ToD sensitivity profiles (Figure S6D). Among the three drugs tested, lorlatinib emerged as the most promising chronotherapeutic candidate, achieving the highest average ToD_{MR} value of 0.61 ± 0.27 (Figure 4H). This cell line- and drug-specific variation in ToD sensitivity is consistent with our previous findings in breast cancer models[22] and reinforced the need for individualized chronotherapeutic assessment.

These experiments provide direct experimental evidence that circadian competence may shape ToD-dependent drug sensitivity in neuroblastoma, highlighting its potential as a determinant of chronotherapeutic efficacy.

DISCUSSION

Circadian clocks are well known to influence cancer progression and treatment response,[18,32,33] yet their function in many tumor types remains unclear. Recently, it has been shown that altered expression of clock genes contribute to tumor development and progression in glioblastoma,[34] which raises questions about circadian regulation in other neural-derived cancers. Neuroblastoma, a highly aggressive pediatric cancer of neural crest origin,[19] represents a particularly relevant context for studying clock function given its severity and developmental origins. Using real-time *Bmal1*- and *Per2* reporters in 12 NB cell models, we uncovered striking heterogeneity in circadian rhythmicity across the cell line panel: most cell lines showed weak or damped rhythms, while only SH-SY5Y and CHP212 were arrhythmic (Figure 2). To our knowledge, these NB cell models have not been evaluated for circadian functionality before, except for GIMEN and SH-SY5Y, which were characterized in our preceding studies.[22] Our findings indicate that complete loss of circadian function is rare. Notably, neither circadian gene expression levels (Figure S5A) nor mutations in core clock genes (none identified across the cell line panel) explains the arrhythmic phenotype, indicating that it may arise from mechanisms including weak intercellular coupling[27] or post-translational and epigenetic regulation of clock proteins.[35] In addition, we observed marked variability in circadian classification across replicates of certain cell lines (Figures 2E–2G), which may be influenced by factors such as the seeding density and synchronization strength.[27,36] We also noted that *Bmal1*- and *Per2* reporter signals sometimes yielded distinct circadian properties within the same cell line, likely reflecting their regulation by different promoter elements and positions within the circadian network, though technical factors such as reporter design may also contribute to these differences. To overcome these limitations of population-based recordings, single-cell approaches using circadian fluorescent reporters[37,38] combined with coupling analyses could offer deeper and more direct insights into the cellular dynamics that underlie circadian regulation in each cell model. In parallel, proteomic approaches focused on post-translational modifications and stability of core clock proteins may reveal molecular defects that contribute to arrhythmic phenotypes.

While intriguing, our exploratory correlations between circadian phenotypes in neuroblastoma cell lines and basic patient characteristics such as age or sex should be interpreted with caution (Figure S2), as long-established cell lines diverge from their parental tumors and lack the microenvironmental cues that shape circadian regulation *in vivo*.[39] Combined with the small sample size, this limits the clinical relevance of such associations. Future studies using patient-derived organoids or xenografts with linked clinical data will be necessary to determine whether circadian phenotypes retain diagnostic value.

Our deep circadian phenotyping approach, employing harmonic regression combined with continuous wavelet transform, revealed significant variability in period, amplitude decay, and overall stability in the circadian signals over time. This is in line with an earlier study where we characterized the circadian clock landscape across numerous breast cancer cell models,[13] suggesting that circadian regulation may be similarly heterogeneous across different cancer types.

It would be valuable to examine circadian behavior in non-malignant, neural crest-derived cells such as trunk neural crest cells (tNCCs), which represent the developmental origin of neuroblastoma. Although we did not identify suitable sources for tNCC cultures for circadian recordings, robust oscillations

(E) Time-of-day response curves (ToD-RCs) for GIMEN (*left*) and SH-SY5Y (*right*) cells treated with lorlatinib (triangle), cisplatin (circle), or doxorubicin (inverted triangle). Responses at each treatment time point are shown relative to treatment at 0 h. The relative response was calculated by dividing the confluency measured 4 days post-treatment by the corresponding confluency of the 0 h treatment. Data points represent the mean ± SD across two independent experiments, each based on 9 images per well.

(F) ToD-RCs for lorlatinib (*left*), cisplatin (*middle*), and doxorubicin (*right*) across five neuroblastoma cell models. Curves show relative responses to ToD 0 h, as described in (E). Cell line markers: GIMEN = triangle; SKNSH = cross; SKNBE(2) = hexagon; SH-SY5Y = diamond; CHP212 = circle. Data points represent the mean across two independent experiments.

(G) ToD variability by cell line, sorted in descending order by average ToD_{MR} values. Points represent individual drug-cell line combinations (drug markers as in (E)). The box edges indicate the 25th and 75th percentiles, with whiskers extending to values within 1.5 times the interquartile range. The median is shown as a red horizontal line.

(H) ToD variability by drug, sorted in descending order by average ToD_{MR} values. The data represent the mean ± SD ToD_{MR} values across cell lines for lorlatinib, cisplatin, and doxorubicin (cell line markers as in (F)).

have been documented in other normal neural cells, including SCN neurons[40] and astrocytes.[41] Direct comparisons between NB and tNCC cells could clarify whether the variable rhythms we detected represent a loss of normal circadian function or mirror a natural diversity potentially present in neural crest progenitor cells.

To assess whether the rhythmic properties of the cell lines have functional growth consequences, we examined their relationship to cell growth parameters. Analysis of the live-cell imaging recordings showed that faster-proliferating lines tended to have weaker or lengthened rhythms (Figure S4), consistent with evidence that clock restoration can act tumor-suppressively in neuroblastoma.[42] Thus, circadian impairment is not only a marker of heterogeneity but seems also to be functionally linked to growth dynamics.

We further asked whether circadian oscillation signatures relate to the cell lines' genetic profiles. Gene expression and LDA analyses showed that small subsets of circadian or NB-specific genes classified phenotypes with high accuracy, whereas larger sets performed poorly. *Bmal1* and *Clock* consistently emerged among circadian predictors, while *Phox2b* and *Ntrk2* stood out among NB-specific ones. However, the precise mechanistic roles of these genes remain unclear, and their predictive value should be validated in larger panels and, ultimately, in patient-derived and *in vivo* models.[43] If confirmed, this approach could enable the determination of a neuroblastoma tumor's circadian clock status from a simple snapshot of gene expression, using either circadian clock genes or neuroblastoma-specific markers. Ultimately, this would have significant implications for patient stratification and the assessment of the benefit from chronotherapeutic strategies.

Finally, given the well-established impact of circadian rhythms in cellular metabolism,[44] proliferation,[45] and drug responsiveness,[46–48] we explored the link between circadian gene expression and drug sensitivity in NB cell lines. Previous work showed that activating the core clock component RORα enhances *Bmal1* expression and increases chemotherapy sensitivity in NB cells.[42] In line with this, our analysis identified several significant correlations between circadian regulators and drug sensitivity (Figure 4A). Notably, topotecan exhibited robust associations across sensitivity metrics, suggesting a circadian-dependent mechanism which is consistent with our earlier findings in breast cancer cell models.[13] Among targeted agents, ALK inhibitors (PF2341066 and TAE684) showed significant associations with circadian genes, highlighting their promise for chronotherapeutic application in neuroblastoma. Furthermore, 17-AAG displayed opposing correlations with *Cry2* and *Clock*, aligning with prior reports of its circadian timing-dependent efficacy[46] and indicating phase-specific relationships within the circadian feedback loop. To validate these findings, future studies should extend drug testing to additional NB models using dynamic assays (e.g., growth rate inhibition with live imaging[49]) and in more complex cancer models such as patient-derived organoids and mouse models. It will also be important to assess whether clinical features (e.g., patient age) or mutation status (e.g., ALK) modulate circadian-drug sensitivity, as our limited dataset suggests that genotype alone does not fully explain the observed variability.

To move beyond correlative evidence, we tested whether circadian competence translates into functional differences in drug response through time-of-day sensitivity assays. Our experiments demonstrate that circadian-competent neuroblastoma models exhibit pronounced temporal variation in drug sensitivity to the ALK inhibitor lorlatinib, the DNA crosslinker cisplatin, and the DNA synthesis inhibitor doxorubicin, while weakly rhythmic lines showed minimal ToD-dependent responses to these drugs. Notably, the relationship between circadian strength and chronotherapeutic potential does not seem to be strictly linear, since the intermediate circadian line SKNBE(2) ranked higher in overall ToD sensitivity than the strongly rhythmic SKNSH (Figure 4G). This suggests that factors beyond circadian component strength influence temporal drug responses, a complexity likely reflecting the interplay of multiple cellular characteristics, including overall drug sensitivity and growth dynamics, which we have previously shown to modulate chronotherapeutic potential in breast cancer models.[22,50] Interestingly, lorlatinib emerged as the most promising chronotherapeutic candidate, which is consistent with our previously identified correlations between circadian gene expression and sensitivity to ALK inhibitors such as PF2341066 (Figure 4A). Taken together, the evidence from both the correlation analyses and the functional experiments highlights the potential of using circadian timing to improve ALK inhibitor therapy in neuroblastoma. Here, validation in patient-derived organoids and *in vivo* models will be essential to better recapitulate tumor temporal dynamics and establish clinically relevant treatment schedules.

While our functional assays demonstrate that circadian heterogeneity is linked to growth dynamics and shapes time-of-day drug sensitivity, further mechanistic studies remain an important future direction. Dissecting how specific circadian gene expression programs translate into rhythmic outputs at the protein and pathway level and clarifying how individual circadian regulators modulate drug responses will be critical to fully understand circadian vulnerabilities in neuroblastoma. Such analyses will likely require single-cell reporter approaches, proteomic profiling of core clock proteins, and expanded time-resolved drug testing in patient-derived models.

In summary, we mapped circadian heterogeneity across neuroblastoma models and showed its relevance for both proliferation and drug response. By linking clock properties to gene expression and drug sensitivity and showing distinct time-of-day drug response dynamics, we establish a framework that underscores the importance of circadian regulation in neuroblastoma. Incorporating circadian profiling into neuroblastoma therapy may enhance efficacy while reducing toxicity,[33] opening new avenues to improve outcomes in this high-risk disease.

Limitations of the study

Our analyses are based on established neuroblastoma cell lines. While these models enable systematic and controlled profiling, they lack important physiological cues present *in vivo* that can influence circadian regulation. This limits the direct clinical relevance of associations between our circadian phenotypes and patient characteristics. While our functional assays demonstrate clear links between circadian competence and time-of-day dependent drug sensitivity, they do not fully resolve the

underlying molecular mechanisms which should be addressed in future mechanistic studies. Arrhythmic phenotypes remain incompletely explained and would benefit from complementary approaches such as single-cell recordings or proteomic profiling of core clock proteins to capture intercellular dynamics and post-translational regulation. Finally, using more complex tumor models will be essential to confirm the translational relevance of our findings and to establish how circadian heterogeneity influences neuroblastoma growth and treatment response in more physiological settings.

RESOURCE AVAILABILITY

Lead contact

Further information and requests should be directed to the lead contact, Adrián E. Granada (adrian@granadalab.org).

Materials availability

This study did not generate new unique reagents.

Data and code availability

- Experimental data have been deposited at Figshare and are publicly available as of the date of publication. Accession numbers are listed in the key resources table.
- All original code has been deposited at GitHub and is publicly available at https://doi.org/10.5281/zenodo.18032430 as of the date of publication.
- Any additional information required to reanalyze the data reported in this paper is available from the lead contact upon request.

ACKNOWLEDGMENTS

We are thankful to Annika Winkler for assistance with sample preparation as well as to Anna-Marie Finger and Astrid Grudziecki for guidance in the bioluminescence recordings. This work is part of a project backed by the German Federal Ministry of Education and Research (BMBF) through the e:Med Juniorverbund DeepLTNBC TP3-01ZX1917C. C.S. received support from the DFG–SCHM 3362/4–1 project number 511886499. J.D. acknowledges support by the Luxembourg National Research Fund (FNR) under the PRIDE program (PRIDE17/12252781).

AUTHOR CONTRIBUTIONS

C.E., C.S., and A.E.G. conceived and planned the study. C.E. performed the experiments. C.E., C.S., J.D., and S.D.L. analyzed the data. A.K. provided resources for the bioluminescence recordings. C.E. wrote the manuscript. A.E.G. acquired funding, supervised the study, and edited the manuscript. All authors contributed to the interpretation of the results, provided critical feedback, and helped shape the research and manuscript.

DECLARATION OF INTERESTS

The authors declare no competing interests.

STAR★METHODS

Detailed methods are provided in the online version of this paper and include the following:

- KEY RESOURCES TABLE
- EXPERIMENTAL MODEL AND STUDY PARTICIPANT DETAILS
  - Cell culture
  - Influence of sex and gender
  - Cell line authentication
- METHOD DETAILS
  - Generation of luciferase reporter cell lines
  - Circadian bioluminescence recordings
  - Long-term live cell imaging
  - Time-of-day drug treatments
  - Experimental design
- QUANTIFICATION AND STATISTICAL ANALYSIS
  - Profiling of circadian signals
  - Principal component analysis-based cluster analysis
  - Expression analysis of circadian genes
  - Linear discriminant analysis
  - Correlation analysis and pairwise linear regression
  - Growth dynamics analysis
  - Parametrization of time-of-day drug response curves

SUPPLEMENTAL INFORMATION

Supplemental information can be found online at https://doi.org/10.1016/j.celrep.2026.116975.

Received: March 19, 2025
Revised: October 15, 2025
Accepted: January 14, 2026

REFERENCES

1. Rosbash, M. (2009). The Implications of Multiple Circadian Clock Origins. PLoS Biol. *7*, e1000062. https://doi.org/10.1371/journal.pbio.1000062.
2. Nikhil, K.L., Korge, S., and Kramer, A. (2020). Heritable gene expression variability and stochasticity govern clonal heterogeneity in circadian period. PLoS Biol. *18*, e3000792. https://doi.org/10.1371/journal.pbio.3000792.
3. Chaix, A., Zarrinpar, A., and Panda, S. (2016). The circadian coordination of cell biology. J. Cell Biol. *215*, 15–25. https://doi.org/10.1083/jcb.201603076.
4. Golombek, D.A., Bussi, I.L., and Agostino, P.V. (2014). Minutes, days and years: molecular interactions among different scales of biological timing. Philos. Trans. R. Soc. Lond. B Biol. Sci. *369*, 20120465. https://doi.org/10.1098/rstb.2012.0465.
5. Takahashi, J.S. (2017). Transcriptional architecture of the mammalian circadian clock. Nat. Rev. Genet. *18*, 164–179. https://doi.org/10.1038/nrg.2016.150.
6. Akman, O.E., Rand, D.A., Brown, P.E., and Millar, A.J. (2010). Robustness from flexibility in the fungal circadian clock. BMC Syst. Biol. *4*, 88. https://doi.org/10.1186/1752-0509-4-88.
7. Zhang, R., Lahens, N.F., Ballance, H.I., Hughes, M.E., and Hogenesch, J.B. (2014). A circadian gene expression atlas in mammals: implications for biology and medicine. Proc. Natl. Acad. Sci. USA *111*, 16219–16224. https://doi.org/10.1073/pnas.1408886111.
8. Chakrabarti, S., and Michor, F. (2020). Circadian clock effects on cellular proliferation: Insights from theory and experiments. Curr. Opin. Cell Biol. *67*, 17–26. https://doi.org/10.1016/j.ceb.2020.07.003.
9. Neufeld-Cohen, A., Robles, M.S., Aviram, R., Manella, G., Adamovich, Y., Ladeuix, B., Nir, D., Rousso-Noori, L., Kuperman, Y., Golik, M., et al. (2016). Circadian control of oscillations in mitochondrial rate-limiting enzymes and nutrient utilization by PERIOD proteins. Proc. Natl. Acad. Sci. USA *113*, E1673–E1682. https://doi.org/10.1073/pnas.1519650113.
10. Sancar, A., Lindsey-Boltz, L.A., Kang, T.H., Reardon, J.T., Lee, J.H., and Ozturk, N. (2010). Circadian clock control of the cellular response to DNA damage. FEBS Lett. *584*, 2618–2625. https://doi.org/10.1016/j.febslet.2010.03.017.
11. Roenneberg, T., and Merrow, M. (2016). The Circadian Clock and Human Health. Curr. Biol. *26*, R432–R443. https://doi.org/10.1016/j.cub.2016.04.011.

12. Fortin, B.M., Mahieu, A.L., Fellows, R.C., Kang, Y., Lewis, A.N., Ead, A.S., Lamia, K.A., Cao, Y., Pannunzio, N.R., and Masri, S. (2025). The diverse roles of the circadian clock in cancer. Nat. Cancer *6*, 753–767. https://doi.org/10.1038/s43018-025-00981-8.

13. Ector, C., Didier, J., De Landtsheer, S., Nordentoft, M.S., Schmal, C., Keilholz, U., Herzel, H., Kramer, A., Sauter, T., and Granada, A.E. (2025). Circadian clock features define novel subtypes among breast cancer cells and shape drug sensitivity. Mol. Syst. Biol. *21*, 315–340. https://doi.org/10.1038/s44320-025-00092-7.

14. Lellupitiyage Don, S.S., Lin, H.H., Furtado, J.J., Qraitem, M., Taylor, S.R., and Farkas, M.E. (2019). Circadian oscillations persist in low malignancy breast cancer cells. Cell Cycle *18*, 2447–2453. https://doi.org/10.1080/15384101.2019.1648957.

15. Maier, B., Wendt, S., Vanselow, J.T., Wallach, T., Reischl, S., Oehmke, S., Schlosser, A., and Kramer, A. (2009). A large-scale functional RNAi screen reveals a role for CK2 in the mammalian circadian clock. Genes Dev. *23*, 708–718. https://doi.org/10.1101/gad.512209.

16. Relógio, A., Thomas, P., Medina-Pérez, P., Reischl, S., Bervoets, S., Gloc, E., Riemer, P., Mang-Fatehi, S., Maier, B., Schäfer, R., et al. (2014). Ras-Mediated Deregulation of the Circadian Clock in Cancer. PLoS Genet. *10*, e1004338. https://doi.org/10.1371/journal.pgen.1004338.

17. Qu, M., Zhang, G., Qu, H., Vu, A., Wu, R., Tsukamoto, H., Jia, Z., Huang, W., Lenz, H.-J., Rich, J.N., and Kay, S.A. (2023). Circadian regulator BMAL1::CLOCK promotes cell proliferation in hepatocellular carcinoma by controlling apoptosis and cell cycle. Proc. Natl. Acad. Sci. USA *120*, e2214829120. https://doi.org/10.1073/pnas.2214829120.

18. Mormont, M.-C., and Levi, F. (2003). Cancer chronotherapy: Principles, applications, and perspectives. Cancer *97*, 155–169. https://doi.org/10.1002/cncr.11040.

19. Louis, C.U., and Shohet, J.M. (2015). Neuroblastoma: molecular pathogenesis and therapy. Annu. Rev. Med. *66*, 49–63. https://doi.org/10.1146/annurev-med-011514-023121.

20. Bosse, K.R., and Maris, J.M. (2016). Advances in the translational genomics of neuroblastoma: From improving risk stratification and revealing novel biology to identifying actionable genomic alterations. Cancer *122*, 20–33. https://doi.org/10.1002/cncr.29706.

21. Ackermann, S., Cartolano, M., Hero, B., Welte, A., Kahlert, Y., Roderwieser, A., Bartenhagen, C., Walter, E., Gecht, J., Kerschke, L., et al. (2018). A mechanistic classification of clinical phenotypes in neuroblastoma. Science *362*, 1165–1170. https://doi.org/10.1126/science.aat6768.

22. Ector, C., Schmal, C., Didier, J., De Landtsheer, S., Finger, A.-M., Müller-Marquardt, F., Schulte, J.H., Sauter, T., Keilholz, U., Herzel, H., et al. (2024). Time-of-day effects of cancer drugs revealed by high-throughput deep phenotyping. Nat. Commun. *15*, 7205. https://doi.org/10.1038/s41467-024-51611-3.

23. Yalçin, M., and Relógio, A. (2023). Sex and age-dependent characterization of the circadian clock as a potential biomarker for physical performance: A prospective study protocol. PLoS One *18*, e0293226. https://doi.org/10.1371/journal.pone.0293226.

24. Talamanca, L., Gobet, C., and Naef, F. (2023). Sex-dimorphic and age-dependent organization of 24-hour gene expression rhythms in humans. Science *379*, 478–483. https://doi.org/10.1126/science.add0846.

25. Schmal, C., Mönke, G., and Granada, A.E. (2022). Analysis of Complex Circadian Time Series Data Using Wavelets. In Circadian Regulation: Methods and Protocols, G. Solanas and P.S. Welz, eds. (Springer US), pp. 35–54. https://doi.org/10.1007/978-1-0716-2249-0_3.

26. Huber, A.L., Papp, S.J., Chan, A.B., Henriksson, E., Jordan, S.D., Kriebs, A., Nguyen, M., Wallace, M., Li, Z., Metallo, C.M., and Lamia, K.A. (2016). CRY2 and FBXL3 Cooperatively Degrade c-MYC. Mol. Cell *64*, 774–789. https://doi.org/10.1016/j.molcel.2016.10.012.

27. Gutu, N., Nordentoft, M.S., Kuhn, M., Ector, C., Möser, M., Finger, A.-M., Heltberg, M.S., Jensen, M.H., Keilholz, U., Kramer, A., et al. (2025). Circadian coupling orchestrates cell growth. Nat. Phys. *21*, 768–777. https://doi.org/10.1038/s41567-025-02838-4.

28. Barretina, J., Caponigro, G., Stransky, N., Venkatesan, K., Margolin, A.A., Kim, S., Wilson, C.J., Lehár, J., Kryukov, G.V., Sonkin, D., et al. (2012). The Cancer Cell Line Encyclopedia enables predictive modelling of anticancer drug sensitivity. Nature *483*, 603–607. https://doi.org/10.1038/nature11003.

29. Ko, C.H., and Takahashi, J.S. (2006). Molecular components of the mammalian circadian clock. Hum. Mol. Genet. *15 Spec No 2*, R271–R277. https://doi.org/10.1093/hmg/ddl207.

30. Lerone, M., Ognibene, M., Pezzolo, A., Martucciello, G., Zara, F., Morini, M., and Mazzocco, K. (2021). Molecular Genetics in Neuroblastoma Prognosis. Children *8*, 456. https://doi.org/10.3390/children8060456.

31. Niemeyer, C., and Eggert, A. (2017). Pädiatrische Hämatologie und Onkologie, 2 Edition (Springer Berlin). https://doi.org/10.1007/978-3-662-43686-8.

32. Sulli, G., Lam, M.T.Y., and Panda, S. (2019). Interplay between Circadian Clock and Cancer: New Frontiers for Cancer Treatment. Trends Cancer *5*, 475–494. https://doi.org/10.1016/j.trecan.2019.07.002.

33. Lévi, F., Okyar, A., Dulong, S., Innominato, P.F., and Clairambault, J. (2010). Circadian Timing in Cancer Treatments. Annu. Rev. Pharmacol. Toxicol. *50*, 377–421. https://doi.org/10.1146/annurev.pharmtox.48.113006.094626.

34. Petkovic, M., Yalçin, M., Heese, O., and Relógio, A. (2023). Differential expression of the circadian clock network correlates with tumour progression in gliomas. BMC Med. Genomics *16*, 154. https://doi.org/10.1186/s12920-023-01585-w.

35. Pacheco-Bernal, I., Becerril-Pérez, F., and Aguilar-Arnal, L. (2019). Circadian rhythms in the three-dimensional genome: implications of chromatin interactions for cyclic transcription. Clin. Epigenetics *11*, 79. https://doi.org/10.1186/s13148-019-0677-2.

36. Finger, A.-M., Jäschke, S., del Olmo, M., Hurwitz, R., Granada, A.E., Herzel, H., and Kramer, A. (2021). Intercellular coupling between peripheral circadian oscillators by TGF-β signaling. Sci. Adv. *7*, eabg5174. https://doi.org/10.1126/sciadv.abg5174.

37. Nagoshi, E., Saini, C., Bauer, C., Laroche, T., Naef, F., and Schibler, U. (2004). Circadian gene expression in individual fibroblasts: cell-autonomous and self-sustained oscillators pass time to daughter cells. Cell *119*, 693–705. https://doi.org/10.1016/j.cell.2004.11.015.

38. Gabriel, C.H., del Olmo, M., Zehtabian, A., Jäger, M., Reischl, S., van Dijk, H., Ulbricht, C., Rakhymzhan, A., Korte, T., Koller, B., et al. (2021). Live-cell imaging of circadian clock protein dynamics in CRISPR-generated knock-in cells. Nat. Commun. *12*, 3796. https://doi.org/10.1038/s41467-021-24086-9.

39. Zaaijer, S., Groen, S.C., and Sanjana, N.E. (2021). Tracking cell lineages to improve research reproducibility. Nat. Biotechnol. *39*, 666–670. https://doi.org/10.1038/s41587-021-00928-1.

40. Abe, M., Herzog, E.D., Yamazaki, S., Straume, M., Tei, H., Sakaki, Y., Menaker, M., and Block, G.D. (2002). Circadian Rhythms in Isolated Brain Regions. J. Neurosci. *22*, 350–356. https://doi.org/10.1523/JNEUROSCI.22-01-00350.2002.

41. Brancaccio, M., Edwards, M.D., Patton, A.P., Smyllie, N.J., Chesham, J.E., Maywood, E.S., and Hastings, M.H. (2019). Cell-autonomous clock of astrocytes drives circadian behavior in mammals. Science *363*, 187–192. https://doi.org/10.1126/science.aat4104.

42. Moreno-Smith, M., Milazzo, G., Tao, L., Fekry, B., Zhu, B., Mohammad, M.A., Di Giacomo, S., Borkar, R., Reddy, K.R.K., Capasso, M., et al. (2021). Restoration of the molecular clock is tumor suppressive in neuroblastoma. Nat. Commun. *12*, 4006. https://doi.org/10.1038/s41467-021-24196-4.

43. Rosselot, A.E., Park, M., Kim, M., Matsu-Ura, T., Wu, G., Flores, D.E., Subramanian, K.R., Lee, S., Sundaram, N., Broda, T.R., et al. (2022). Ontogeny and function of the circadian clock in intestinal organoids. EMBO J. *41*, e106973. https://doi.org/10.15252/embj.2020106973.

44. Bass, J., and Takahashi, J.S. (2010). Circadian Integration of Metabolism and Energetics. Science *330*, 1349–1354. https://doi.org/10.1126/science.1195027.

45. Matsuo, T., Yamaguchi, S., Mitsui, S., Emi, A., Shimoda, F., and Okamura, H. (2003). Control mechanism of the circadian clock for timing of cell division in vivo. Science *302*, 255–259. https://doi.org/10.1126/science.1086271.

46. Lee, Y., Fong, S.Y., Shon, J., Zhang, S.L., Brooks, R., Lahens, N.F., Chen, D., Dang, C.V., Field, J.M., and Sehgal, A. (2021). Time-of-day specificity of anticancer drugs may be mediated by circadian regulation of the cell cycle. Sci. Adv. *7*, eabd2645. https://doi.org/10.1126/sciadv.abd2645.

47. Ye, Y., Xiang, Y., Ozguc, F.M., Kim, Y., Liu, C.-J., Park, P.K., Hu, Q., Diao, L., Lou, Y., Lin, C., et al. (2018). The Genomic Landscape and Pharmacogenomic Interactions of Clock Genes in Cancer Chronotherapy. Cell Syst. *6*, 314–328.e2. https://doi.org/10.1016/j.cels.2018.01.013.

48. Dallmann, R., Brown, S.A., and Gachon, F. (2014). Chronopharmacology: New Insights and Therapeutic Implications. Annu. Rev. Pharmacol. Toxicol. *54*, 339–361. https://doi.org/10.1146/annurev-pharmtox-011613-135923.

49. Hafner, M., Niepel, M., Chung, M., and Sorger, P.K. (2016). Growth rate inhibition metrics correct for confounders in measuring sensitivity to cancer drugs. Nat. Methods *13*, 521–527. https://doi.org/10.1038/nmeth.3853.

50. Gutu, N., Ishikuma, H., Ector, C., Keilholz, U., Herzel, H., and Granada, A.E. (2025). A combined mathematical and experimental approach reveals the drivers of time-of-day drug sensitivity in human cells. Commun. Biol. *8*, 491. https://doi.org/10.1038/s42003-025-07931-1.

51. Balsalobre, A., Brown, S.A., Marcacci, L., Tronche, F., Kellendonk, C., Reichardt, H.M., Schütz, G., and Schibler, U. (2000). Resetting of Circadian Time in Peripheral Tissues by Glucocorticoid Signaling. Science *289*, 2344–2347. https://doi.org/10.1126/science.289.5488.2344.

52. Berlak, M., Tucker, E., Dorel, M., Winkler, A., McGearey, A., Rodriguez-Fos, E., da Costa, B.M., Barker, K., Fyle, E., Calton, E., et al. (2022). Mutations in ALK signaling pathways conferring resistance to ALK inhibitor treatment lead to collateral vulnerabilities in neuroblastoma cells. Mol. Cancer *21*, 126. https://doi.org/10.1186/s12943-022-01583-z.

53. Xu, Z., Sun, Y., Wang, D., Sun, H., and Liu, X. (2020). SNHG16 promotes tumorigenesis and cisplatin resistance by regulating miR-338-3p/PLK4 pathway in neuroblastoma cells. Cancer Cell Int. *20*, 236. https://doi.org/10.1186/s12935-020-01291-y.

54. Lautz, T.B., Jie, C., Clark, S., Naiditch, J.A., Jafari, N., Qiu, Y.-Y., Zheng, X., Chu, F., and Madonna, M.B. (2012). The Effect of Vorinostat on the Development of Resistance to Doxorubicin in Neuroblastoma. PLoS One *7*, e40816. https://doi.org/10.1371/journal.pone.0040816.

55. Mönke, G., Sorgenfrei, F.A., Schmal, C., and Granada, A.E. (2020). Optimal time frequency analysis for biological data - pyBOAT. Preprint at bioRxiv. https://doi.org/10.1101/2020.04.29.067744.

56. Leise, T.L., and Harrington, M.E. (2011). Wavelet-based time series analysis of circadian rhythms. J. Biol. Rhythms *26*, 454–463. https://doi.org/10.1177/0748730411416330.

57. Myung, J., Schmal, C., Hong, S., Tsukizawa, Y., Rose, P., Zhang, Y., Holtzman, M.J., De Schutter, E., Herzel, H., Bordyugov, G., and Takumi, T. (2018). The choroid plexus is an important circadian clock component. Nat. Commun. *9*, 1062. https://doi.org/10.1038/s41467-018-03507-2.

58. Westermark, P.O., Welsh, D.K., Okamura, H., and Herzel, H. (2009). Quantification of Circadian Rhythms in Single Cells. PLoS Comput. Biol. *5*, e1000580. https://doi.org/10.1371/journal.pcbi.1000580.

59. Schmal, C., Herzog, E.D., and Herzel, H. (2018). Measuring Relative Coupling Strength in Circadian Systems. J. Biol. Rhythms *33*, 84–98. https://doi.org/10.1177/0748730417740467.

STAR★METHODS

KEY RESOURCES TABLE

REAGENT or RESOURCE	SOURCE	IDENTIFIER
Bacterial and virus strains		
Lentivirus for transduction	This paper. From HEK293T cells using pAB-mBmal1:Luc-Puro or plenti6-mPer2:Luc-Blas together with psPAX2 and pMD2G (see section "Recombinant DNA").	–
Chemicals, peptides, and recombinant proteins		
RPMI-1640 medium	Gibco	Cat #21875091
Fetal Bovine Serum (FBS)	Gibco	Cat #10270106
Penicillin-Streptomycin (Pen-Strep)	Gibco	Cat #15140122
FluoroBrite DMEM medium (phenol red free)	Gibco	Cat #A1896701
L-Glutamine (200 mM)	Gibco	Cat #25030-024
HEPES (1 M)	Gibco	Cat #15630056
Lipofectamine 3000	Invitrogen	Cat #L3000001
Protamine sulfate (10 G)	Sigma	Cat #P3369
PBS pH 7.4	Gibco	Cat #10010056
Blasticidin S HCl	Adooq	Cat #A14212
Puromycin	Gibco	Cat #A1113803
Dexamethasone	Sigma	Cat #D4902
D-Luciferin	Abmole	Cat #M9053
Lorlatinib	Sigma	Cat #PZ0039
Cisplatin	Sigma	Cat #232120
Doxorubicin	Hölzel	Cat #A14403-100
Dimethyl sulfoxide (DMSO)	Sigma	Cat #D8418
Deposited data		
Circadian luciferase data	This paper	Figshare: https://doi.org/10.6084/m9.figshare.30815522
Growth and time-of-day-dependent drug response data	This paper	Figshare: https://doi.org/10.6084/m9.figshare.30815537
Drug sensitivity data	Cancer Cell Line Encyclopedia (CCLE), 2022-Q2	CCLE: https://sites.broadinstitute.org/ccle/datasets
Gene expression data	Cancer Cell Line Encyclopedia (CCLE), 2022-Q2	CCLE: https://sites.broadinstitute.org/ccle/datasets
Experimental models: Cell lines		
Neuroblastoma cell lines (CHP212, CLBGA, GIMEN, IMR5, KELLY, LAN5, NGP, SH-SY5Y, SKNAS, SKNBE(1), SKNBE(2), SKNSH)	Johannes Schulte, Universitätsklinikum Tübingen, Clinic for Pediatrics and Adolescent Medicine, Germany	N/A
HEK293T	Galit Lahav, Harvard Medical School, Department of Systems Biology, USA	N/A
Bmal1-Luc reporter cell lines	This paper	N/A
Per2-Luc reporter cell lines	This paper	N/A
Recombinant DNA		
pAB-mBmal1:Luc-Puro	Achim Kramer, Laboratory of Chronobiology, Charité – Universitätsmedizin Berlin, Germany	N/A

(*Continued on next page*)

Continued		
REAGENT or RESOURCE	SOURCE	IDENTIFIER
plenti6-mPer2:Luc-Blas	Achim Kramer, Laboratory of Chronobiology, Charité – Universitätsmedizin Berlin, Germany	N/A
psPAX2	Addgene	ID 12260
pMD2G	Addgene	ID 12259
Software and algorithms		
Analysis pipelines	This paper	https://doi.org/10.5281/zenodo.18032430
Python v3.9.7	N/A	N/A
Python Spyder v5.4.5	N/A	N/A
pyBOAT (Python package)	Mönke et al.[51]	https://github.com/tensionhead/pyBOAT
pywt	Lee et al.[52]	https://github.com/PyWavelets/pywt
seaborn v0.13.2	Waskom et al.[53]	N/A
statsmodels v0.13.2	Seabold et al.[54]	https://github.com/statsmodels/statsmodels
SciPy v1.13.1	Virtanen et al.[55]	https://github.com/scipy/scipy
Scikit-Learn v1.1.1	Pedregosa et al.[56]	https://github.com/scikit-learn/scikit-learn
PyCharm Community Edition v2021.2.2	N/A	N/A
Incucyte software	Essen BioScience	N/A
MATLAB v2024b	N/A	N/A
Anaconda Navigator v2.5.0	N/A	N/A
Other		
LumiCycle luminometer	Actimetrics	N/A
Incucyte SX5	Essen BioScience	N/A

EXPERIMENTAL MODEL AND STUDY PARTICIPANT DETAILS

Cell culture

All neuroblastoma cell lines (CHP212, CLBGA, GIMEN, IMR5, KELLY, LAN5, NGP, SH-SY5Y, SKNAS, SKNBE(1), SKNBE(2), SKNSH) were kindly provided by the Schulte lab (Universitätsklinikum Tübingen, Clinic for Pediatrics and Adolescent Medicine, Germany). Clinical characteristics of the patients from whom each cell line was derived were as follows [CELL LINE: age (years) | gender (Male/Female)]: CHP212: 1.8y |M; CLBGA: 4y |M; GIMEN: 3.5y |F; IMR5: 1.1y |M; KELLY: 1y |F; LAN5: 0.4y |M; NGP: 2.6y |M; SH-SY5Y: 4y |F; SKNAS: 8y |F; SKNBE(1): 1.7y |M; SKNBE(2): 2.2y |M; SKNSH: 4y |F. Patient ages at sample collection ranged from 0.4 to 8 years (median 2.4 years). Five cell lines were derived from female patients and seven from male patients. The cell lines exhibited diverse genetic backgrounds including MYCN amplification status (amplified $n = 9$, normal $n = 3$) and various mutations in ALK, TP53, PHOX2B and ATRX genes. All clinical information can be derived from Table S1. All twelve cell lines were included in the circadian rhythm profiling experiments and no experimental groups were allocated.

Cells were cultured in RPMI-1640 medium (Gibco) supplemented with 10% fetal bovine serum (FBS, Gibco) and 1% penicillin-streptomycin (Pen-Strep, Gibco). For bioluminescence measurements, the medium was switched to a phenol red-free FluoroBrite DMEM medium (Gibco), supplemented with 10% FBS, 300 mg/L L-glutamine (Gibco) and 1% Pen-Strep. Cell cultures were maintained at 37°C with 5% CO_2.

Influence of sex and gender

Circadian rhythms exhibit sex- and age-dependent variation in humans. Biological sex influences circadian clock function through hormonal regulation and sex-specific gene expression patterns.[23,24] Age-related changes in circadian regulation have also been documented,[24] however, the retention of such associations in long-established cancer cell lines cultured *in vitro* remains uncertain, as these models lack the hormonal and microenvironmental contexts present *in vivo*.

Cell line authentication

All cell lines were routinely tested for mycoplasma contamination by PCR and tested negative. The cell lines have not been explicitly authenticated, i.e., by short tandem repeat profiling, by the authors.

METHOD DETAILS

Generation of luciferase reporter cell lines

HEK293T cells (kindly provided by the Lahav lab, Harvard Medical School, Department of Systems Biology, USA) at approximately 80% confluency were maintained in RPMI-1640 medium supplemented with 10 mM HEPES and transfected using a mixture that included 8.4 μg of a lentiviral expression plasmid (either pAB-mBmal1:Luc-Puro or plenti6-mPer2:Luc-Blas), 6 μg of psPAX2 (Addgene #12260) and 3.6 μg of pMD2G (Addgene #12259) to generate lentivirus encoding circadian luciferase reporters. Transfection was conducted with Lipofectamine 3000 (Invitrogen) following the manufacturer's protocol. Viral particles were collected and filtered through 0.45 μm Millipore filters at both 48- and 72-h post-transfection. For the transduction process, target cells at around 70% confluency were exposed for 6 h to a mixture containing 1 mL of the lentivirus-containing supernatant, 8 μg/mL protamine sulfate (Sigma) and 10 μM HEPES (Gibco). After incubation, cells were washed with PBS (Gibco) and maintained in their standard culture medium. Two days later, antibiotic selection was initiated by adding either 5 μg/mL blasticidin (Adooq) or 2 μg/mL puromycin (Gibco), according to the resistance marker encoded in the lentiviral vector.

Circadian bioluminescence recordings

Bmal1 or *Per2* luciferase reporter cell lines were seeded into 35-mm dishes (Nunc) so that they reached confluence by the following day. To synchronize the circadian rhythms across individual cells, a 1 μM dose of dexamethasone[36,51] (Sigma, prepared in EtOH) was applied. After a 30-min incubation, the cells were rinsed once with PBS and imaging medium containing 250 μM D-Luciferin (Abmole) was added. The dishes were then sealed with parafilm to prevent evaporation during the bioluminescence recording period. Measurements were taken every 10 min for up to 6 days using an incubator-embedded luminometer (LumiCycle, Actimetrics).

Long-term live cell imaging

Live-cell imaging experiments were performed using cells expressing the *Bmal1*-Luc reporter where available. Cells were seeded in 48-well plates (Falcon) at densities reaching confluence by experiment termination. One day post cell seeding, long-term imaging was conducted using an Incucyte live-cell widefield microscope (Essen BioScience) with environmental control. Brightfield images were acquired at 10× magnification from 9 fields per well at 2-h intervals over 5 days. Confluency detection was performed using integrated Incucyte software, with subsequent data analysis in Python.

Time-of-day drug treatments

Cells were seeded at densities reaching confluence by experiment termination and allowed to adhere overnight. The following day, live recordings were initiated as described above. To generate distinct circadian populations, independent resetting steps were performed every 4 h over an 8-h window, yielding cohorts at 0, 4 and 8 h circadian time. Each group was subsequently treated with the same drug concentration, corresponding to the approximate half-maximal effective concentration (EC_{50}) to appreciate response differences, either 32 or 48 h after the initial reset and cell growth was monitored for 4 days to determine sensitivity. This setup enabled simultaneous assessment of six circadian stages (0, 4, 8, 16, 20 and 24 h). Drug concentrations were selected based on literature values and partially adjusted in the second experiment to reduce toxicity. In the first experiment, lorlatinib (Sigma) was applied at 50 nM,[52] cisplatin (Sigma) at 1.5 μM[53] and doxorubicin (Hölzel) at 20 nM.[54] In the second experiment, lorlatinib was increased to 100 nM for GIMEN, SKNBE(2) and CHP212, while SH-SY5Y and CHP212 were treated with 1 μM cisplatin and 10 nM doxorubicin. All drugs were administered in 0.18% DMSO (Gibco) as solvent.

Experimental design

Unless stated otherwise all experiments were performed using 2–3 biological replicates with 2–3 technical replicates per condition. Exact numbers of biological and technical replicates and total sample sizes for each cell line and reporter are specified in the corresponding figure legends. Sample sizes were based on prior circadian bioluminescence studies demonstrating adequate power to detect rhythm changes in e.g., phase shifts and amplitude changes and practical constraints including experimental throughput. Data acquisition and analysis were not performed blinded due to the nature of the experimental setup and predefined reporter and treatment conditions. For time-of-day treatment assays, randomization was not applied as treatment groups were defined by fixed circadian time points and cell line identity.

QUANTIFICATION AND STATISTICAL ANALYSIS

Profiling of circadian signals

Data pre-processing

Each individual time series was trimmed to a length of 136 h and 10 min (i.e., approx. 5.67 days) so that all recordings were of equal size for a better quantitative comparability. Due to strong non-linear baseline-expression trends the trimmed time series were subsequently detrended by a sinc-filter with cutoff period T_c = 48 h using the *sinc_smooth* function of the Python package *pyBOAT* as previously described.[25,55] Due to a strong startle response at the beginning of the recordings, the first 5h of the recordings are neglected throughout the whole time series analysis.

Multiresolution analysis

A discrete wavelet transform based multiresolution analysis (MRA) was applied to determine the circadian rhythmicity of the detrended time series as previously described.[56,57] Here, the original signal is decomposed into its contributions at different period bands, termed details. The sum of all details equals the original signal. By this means, the MRA partitions the variance of the signal along the difference details, i.e., period bands. Thus, the portion of the variance corresponding to the part of the signal within the circadian range can be quantified and has been used as a measure of circadian rhythmicity.[56,57] We implemented the MRA using a Daubechies 20 wavelet (*db20*) of the Python *pywt* library and deconstructed the original signal into 7 details. To obtain a detail with a proper circadian period range between [16h, 32h], detrended time series have been down sampled from dt = 10 to dt = 30 min.

Nonlinear least square fitting

To determine the damping coefficients together with the period, initial amplitude and noise strength of the oscillations, we fitted a stochastic linearly damped oscillator to the individual time-detrended time series using an autocorrelation approach as described previously.[58,59] In a nutshell, the autocorrelation function of a stochastic linearly damped oscillator can be determined analytically and this analytically obtained function is fitted to the autocorrelation of the experimentally obtained time series.[59] The autocorrelation of the experimental time series is obtained via the *acovf* function of the *statsmodels* Python library. The non-linear least squares fit of autocorrelation function of the stochastic linearly damped oscillator model to the experimentally obtained autocorrelation has been done by means of the *curve_fit* function of the Scientific Python (*Scipy*) module. Only traces classified as *circadian* or *mixed* in the preceding multiresolution analysis were included. To ensure circadian relevance, time series with fitted periods >36 h were excluded.

Continuous wavelet transform

To determine non-stationary properties of the experimental time series, we applied a continuous wavelet transform (CWT) as implemented within the *pyBOAT* Python package.[25,55] Periods, phases and amplitudes are evaluated along the connected line of points of maximal power, termed *ridge*. For ridge detection, a threshold of 20 (arbitrary units of the CWT power spectrum) was applied to filter out low-amplitude fluctuations and ensure that only robust oscillatory components are considered.[55] Periods and phases were extracted by analyzing the amplitude-normalized signal within the continuous wavelet transform (CWT) power spectrum, while amplitudes and ridge lengths were evaluated from amplitude-unnormalized signals. Only traces classified as *circadian* or *mixed* in the preceding multiresolution analysis were analyzed.

Principal component analysis-based cluster analysis

A principal component analysis (PCA)-based dimensionality reduction was done via the *Scikit-Learn* class *PCA*. Values of the first two principal components were used to group the data into four clusters using the k-means algorithm, implemented via the *Scikit-Learn* class *KMeans*. Based on this classification, we selected only the samples within the mixed or circadian clusters for further analysis, even when samples of the same cell line fell into different clusters, e.g., mixed and infradian.

Expression analysis of circadian genes

Gene expression data of core circadian clock genes were retrieved from the CCLE (DepMap 2022-Q2): https://sites.broadinstitute.org/ccle/datasets. Cell models were clustered according to their expression levels of core circadian clock genes using the *clustermap* function from the *seaborn* Python library, applying *Euclidean distance* and *complete linkage* for clustering.

Linear discriminant analysis

Linear discriminant analysis was performed on the min-max scaled gene expression of 16 circadian clock genes and 11 NB-related genes, reducing the data complexity to a single dimension. The continuous target drug sensitivity vectors for this supervised approach were binarized in respect to their median sensitivities. The *LinearDiscriminantAnalysis* class from the *scikit-learn* Python library was used with default tolerance parameter of 0.0001. Beyond the full sets of 16 circadian and 11 NB-related genes, LDA was applied to multiple gene subsets and evaluated using the log10-transformed ratio of between-to within-cluster-distances (BCD/WCD). The robustness of each model was further assessed by leave-one-out cross-validation (LOOCV), implemented with the *model_selection* module of *scikit-learn* (Python v3.9.7) in PyCharm Community Edition (v2021.2.2).

Correlation analysis and pairwise linear regression

Spearman's rank correlation was used to assess the relationship between circadian gene expression and the drug sensitivity parameters ActArea, IC_{50} and EC_{50}. The correlations were clustered using the *clustermap* function from the *seaborn* Python library, applying *Euclidean distance* and *complete linkage* for clustering. Statistical significance of correlations was determined using a two-sided *t* test with no adjustments made for multiple comparisons in the initial analysis. Significance levels are indicated by asterisks: * p-value = 0.037, *** p-value = 1.4×10^{-24}. To control for multiple comparisons, the Bonferroni correction method was applied, leaving four significant correlations with $Bf_{adj\_p} = 1.6 \times 10^{-4}$. Pairwise linear regression was performed to visualize significant correlations between single gene expression and drug sensitivity using the *lmplot* and *regplot* functions from the *seaborn* Python library with a confidence interval of 95%.

Growth dynamics analysis

One day after seeding, cell proliferation was monitored by long-term live-cell imaging of confluency as described above. Raw confluence trajectories were averaged across 9 images per well, smoothed with a Savitzky-Golay filter (window = 5 frames, polynomial order = 2), normalized to the initial timepoint, and truncated to 92 h. These processed growth curves were fitted with a logistic growth function:

$$\text{Growth}(t) = \frac{L}{1 + e^{(-k(t - t_0)}} \quad \text{(Equation 1)}$$

where L is the carrying capacity, k is the growth rate constant, and t_0 is the inflection point. Non-linear least squares optimization (curve_fit, SciPy v1.7.1) was used to extract growth parameters. For correlation analyses, growth rates were systematically compared with circadian parameters obtained from MRA, CWT and ACoF. Pearson correlation coefficients were computed and significant associations were visualized using linear regression fits. Two cell lines were excluded from growth dynamics analysis: LAN5 due to compromised cell viability post-thaw and KELLY due to poor plate adherence that resulted in an insufficient cell density for reliable growth quantification.

Parametrization of time-of-day drug response curves

Drug response data from the time-of-day treatment experiments were averaged across nine images per well. The final confluency, measured four days after treatment ("final response"), was normalized to the confluency at the respective treatment timepoint. Time-of-day response curves (ToD-RCs) were generated by averaging the final responses of each treatment timepoint across two independent experiments (Figure 4), normalizing them to the 0 h response and interpolating the resulting values using piecewise cubic hermite interpolation (PCHIP). In Figure S6C, ToD-RCs are shown separately for each experiment to illustrate reproducibility. To quantify temporal modulation, the maximum ToD response range (ToD_{MR}) was calculated as the difference between the highest and lowest relative responses across circadian timepoints. To quantify inter-experimental variability for each cell line, the coefficient of variation (*coeff. var.*) was calculated at each timepoint across both experiments, then aggregated by drug and subsequently by cell model.

Cell Reports, Volume *45*

Supplemental information

Circadian rhythm heterogeneity modulates drug response variations in neuroblastoma models

Carolin Ector, Christoph Schmal, Jeff Didier, Sébastien De Landtsheer, Johannes H. Schulte, Ulrich Keilholz, Thomas Sauter, Achim Kramer, Hanspeter Herzel, and Adrián E. Granada

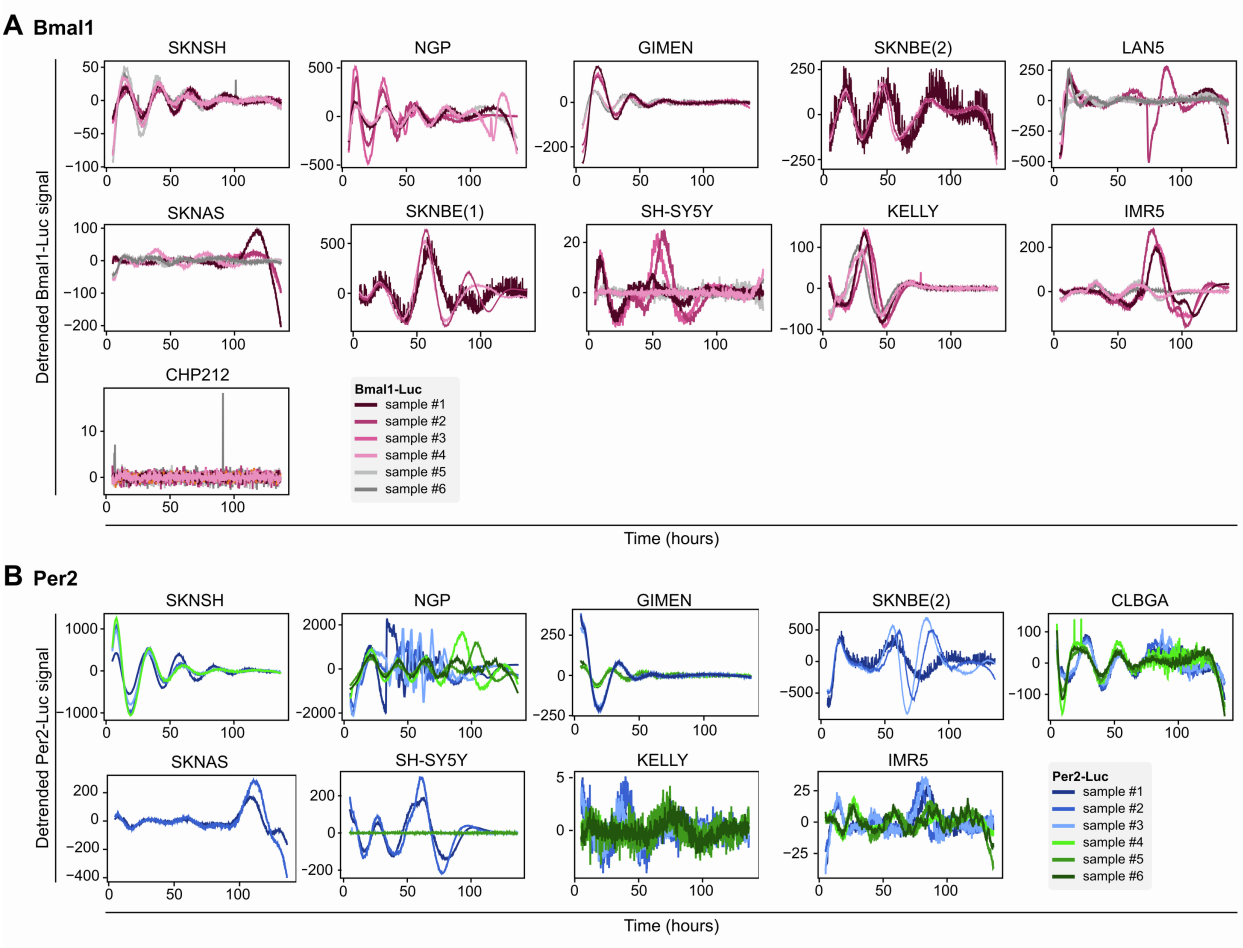

Figure S1. Real-time circadian luciferase signals across neuroblastoma cell lines, Related to Figure 1.

(**A**) Detrended *Bmal1*-Luc signals from neuroblastoma cell lines, with replicates overlaid and distinguished by distinct colors. NB cell lines were assayed in two biological replicates á technical triplicates (*n*=6 samples). NGP was assayed in technical duplicates in one of the experiments (*n*=5). CHP212 was assayed in three biological replicates á technical triplicates (*n*=9). SKNBE(1) and SKNBE(2) was assayed in a single experiment á technical triplicates (*n*=3).

(**B**) Detrended *Per2*-Luc signals from neuroblastoma cell lines, with replicates overlaid and distinguished by distinct colors. Cell lines were assayed in two biological replicates á technical triplicates (*n*=6 samples). SH-SY5Y was assayed in technical duplicates in one of the experiments (*n*=5). SKNSH was assayed in a single sample in one of the experiments (*n*=4). GIMEN and SKNBE(2) was assayed in a single experiment á technical triplicates (*n*=3). SKNAS was assayed in a single experiment in technical duplicates (*n*=2).

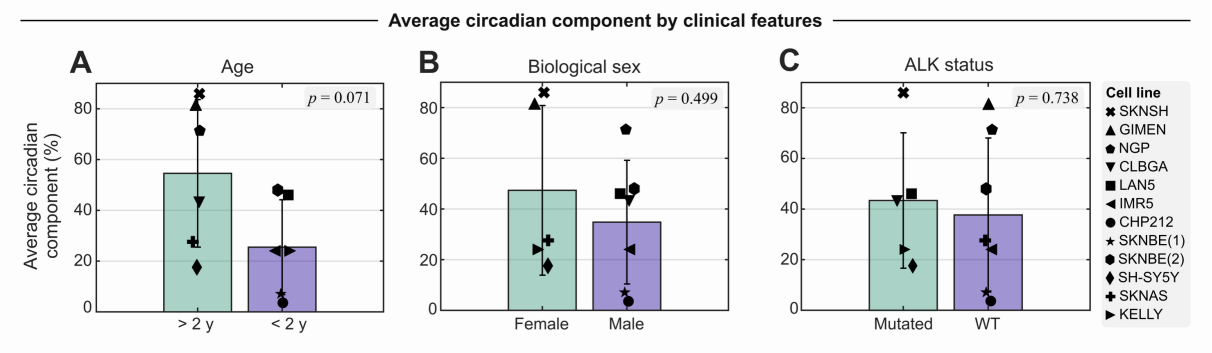

Figure S2. Circadian components in neuroblastoma cell models stratified by clinical features, Related to Figure 1.

(**A**) Bar diagram of MRA circadian components in neuroblastoma cell lines, stratified by patient age: patients aged >2 years (green, *n*=6) vs. <2 years (purple, *n*=6). Bars represent the mean±s.d., with individual cell lines overlaid as scatter plot. Group differences were evaluated using a two-sided *t*-test with no adjustments made, with *p*=0.071.

(**B**) See **A**, here stratified by patient biological sex: female (green, *n*=5) vs. male (purple, *n*=7). *p*=0.499.

(**C**) See **A**, here stratified by patient ALK status: mutated (green, *n*=5) vs. wild-type ("WT", purple, *n*=7). *p*=0.738

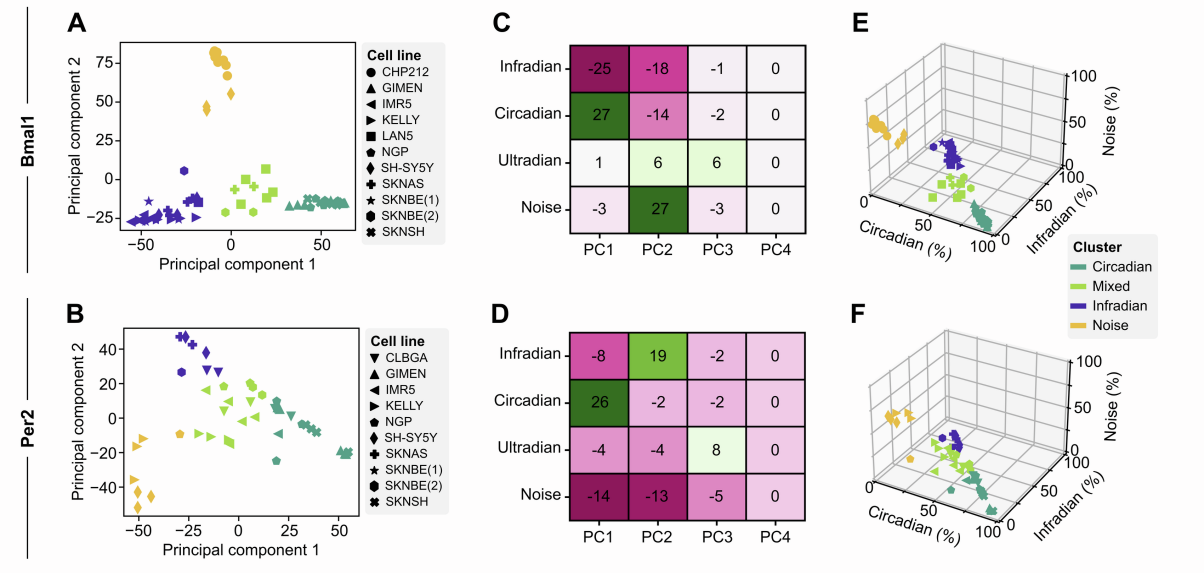

Figure S3. *Bmal1*- and *Per2*-specific cluster analysis of neuroblastoma cell lines, Related to Figure 1.

(**A**) Principal component analysis (PCA) biplot showing the distribution of all *Bmal1*-NB cell line samples (*n*=62) along the first two principal components, calculated from the four MRA frequency components. Cell models are distinguished by markers, and PCA clusters are outlined and color-coded for clarity.

(**B**) See **A**, but for *Per2*-Luc cell line samples (*n*=44).

(**C**) Heatmap of the contributions of each MRA frequency components to the PCA shown in **A**, including PC3 and PC4. Color intensity and values indicate the magnitude and direction of contributions, with positive values in green and negative values in pink to purple.

(**D**) See **C**, here corresponding to the PCA shown in **B** (*Per2*-Luc analysis).

(**E**) 3D scatter plot depicting the distribution of all *Bmal1*-Luc samples along the MRA circadian, infradian, and noise axes. Clusters, determined by the dominant signal components, are color-coded for clarity.

(**F**) See **E**, but for *Per2*-Luc cell line samples.

Data shown in **A–F** is derived from two biological replicates á technical triplicates (*n*=6 samples per Luc-reporter). NGP-*Bmal1* and SH-SY5Y-*Per2* were assayed in technical duplicates in one experiment (*n*=5). CHP212-*Bmal1* was assayed in three biological replicates á technical triplicates (*n*=9). GIMEN-*Per2* were assayed in a single experiment á technical triplicates (*n*=3). SKNSH-*Per2* was assayed in a single sample in one experiment (*n*=4). SKNAS-*Per2*, SKNBE(1) and SKNBE(2) was assayed in a single experiment in technical duplicates (*n*=2).

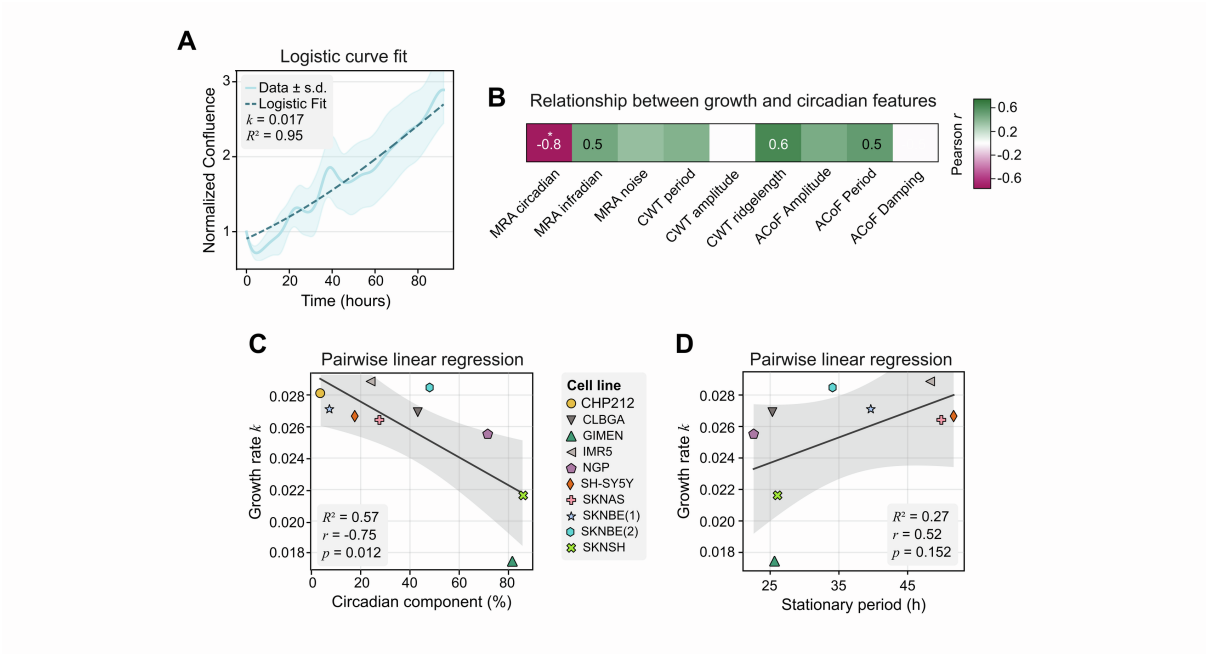

Figure S4. Circadian weakness and prolonged circadian periods associate with faster neuroblastoma growth, Related to Figure 2.

(**A**) Representative logistic curve fit of GIMEN confluence data from long-term live-cell imaging. Raw data was normalized and fitted to a logistic growth model to extract growth rates (*k*). Data represent the mean±s.d. across 9 individual images per well.

(**B**) Pearson correlation matrix between circadian oscillation parameters and growth rates across the neuroblastoma panel. Only correlations with absolute values ≥ 0.5 are displayed; asterisk indicate p=0.012. n=10 cell lines for MRA parameters; n=9 for ACoF parameters; n=7 for CWT parameters.

(**C**) Linear regression between growth rates and MRA circadian components across 10 NB cell lines, with the shaded area representing the 95% confidence interval. R^2 values indicate model fit, r and p the Pearson correlation coefficient and significance, respectively.

(**D**) See C, shown for the relationship between growth rates and stationery (ACoF) circadian periods across 9 NB cell lines.

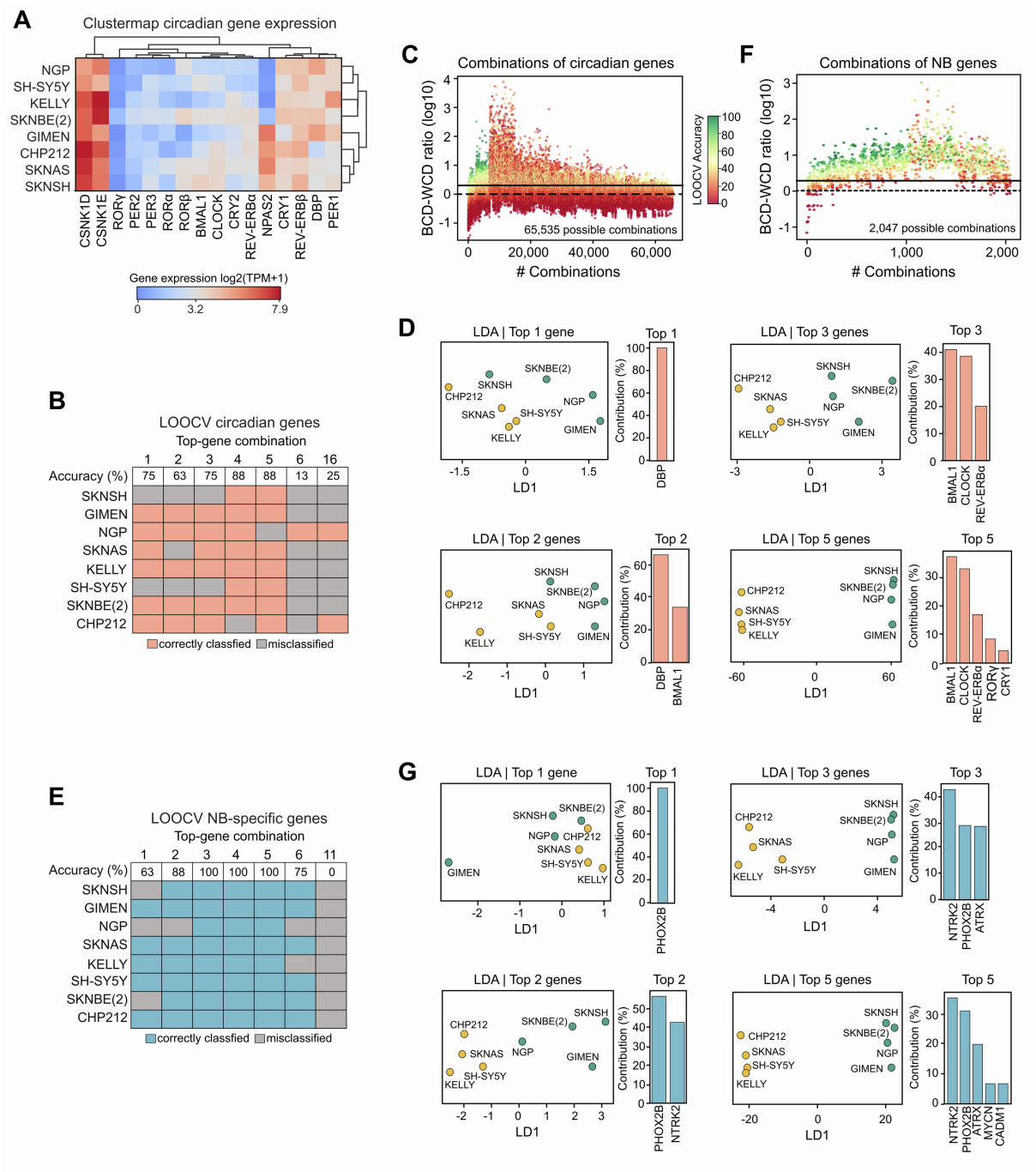

Figure S5. LDAs of the top-performing gene combinations to predict circadian phenotypes, Related to Figure 3.

(**A**) Cluster map of neuroblastoma cell models based on core clock gene expression values, generated using the Euclidean distance method.

(**B**) LOOCV results on top-performing circadian gene combinations of up to 6 genes, and the entire set of circadian genes, corresponding to panel **C** and **Fig. 3B** of the main article. The color coding indicates each cell line's correct (orange) or incorrect (gray) classification, and the top row shows the overall LOOCV accuracy (in %) per drug. *n*=8 cell line models.

(**C**) All possible combinations of circadian genes plotted against their corresponding log10 ratio of between-cluster distance (BCD) to within-cluster distance (WCD), an LDA-based metric of separation quality. The color-coding denotes the corresponding predictive accuracy of each gene combination, as determined by leave-one-out cross-validation (LOOCV).

(**D**) *Left panels:* LDA on median-binarized circadian components (determined via MRA), using the top-1/-2/-3/-5 performing circadian genes as predictors. Cell models with circadian components below or above the median are shown in yellow and green, respectively. The x-axis represents the first linear discriminant (LD1), reflecting the greatest variance between these two groups. *Right panels:* Bar plot rankings of the corresponding gene combinations by their individual contribution to the discriminative power of the LDA model.

(**E**) See **B**, here shown for LDA on NB-specific genes.

(**F**) see **C**, here shown for all possible combinations of neuroblastoma (NB)-specific genes.

(**G**) See **D**, here shown for top performing NB-specific genes as predictors.

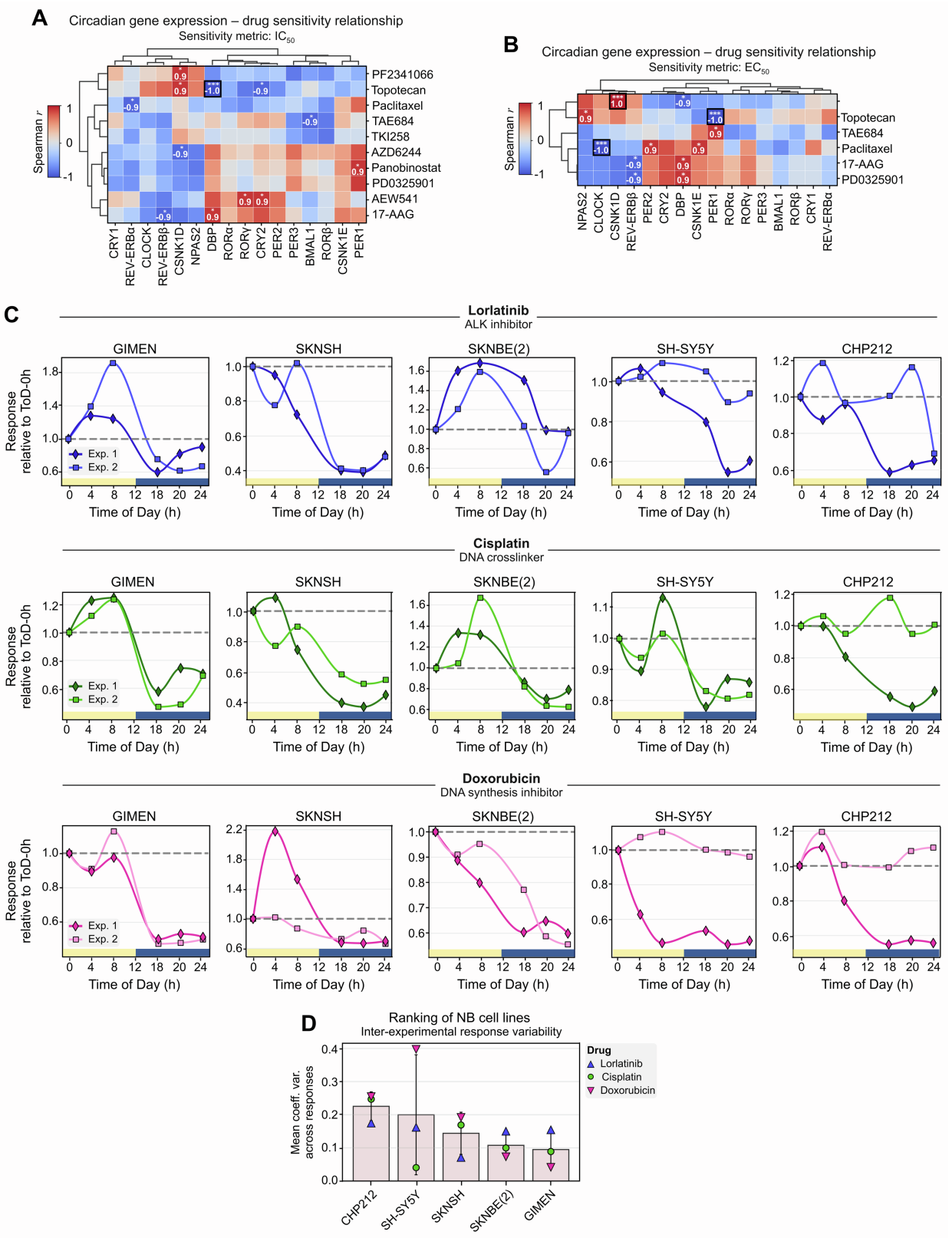

Figure S6. Complementary circadian gene-drug associations and experimental evidence for ToD-dependent drug responses, Related to Figure 4.

(**A**) Cluster map of Spearman correlation coefficients between IC_{50} values for multiple drugs and circadian clock gene expression in neuroblastoma, based on CCLE data. Significant correlations (two-sided *t*-test with no adjustments made) are indicated by stars, where * denotes *p*-values=0.037 and ***

p-values=$1.4x10^{-24}$. Those correlations remaining significant after Bonferroni correction ($Bf_{adj\_p}=1.6x10^{-4}$) are outlined in black.

(**B**) See **A**, here shown for EC_{50} values. * denotes *p*-values=0.037 and *** *p*-values=$1.4x10^{-24}$. Those correlations remaining significant after Bonferroni correction ($Bf_{adj\_p}=1.6x10^{-4}$) are outlined in black.

(**C**) ToD-RCs for each cell line-drug combination, corresponding to **Figures 4E** and **4F** of the main manuscript. Results are shown for two independent experiments (Experiment 1=circles; Experiment 2=triangles), each based on 9 images per well.

(**D**) Inter-experimental response variability by cell line. Barplots showing the mean±s.d. coefficient of variation (coeff. var.) of ToD responses between experiment 1 and 2, aggregated across drugs for each cell line. Drug markers: lorlatinib (triangle), cisplatin (circle), doxorubicin (inverted triangle).

Table S1: Clinical characteristics of the patients from whom each neuroblastoma cell line model was derived, Related to Figure 1.
Clinical characteristics compiled from Thiele, 2002[1] and Barretina et al., 2012[2].

Cell line	Clinical characteristics of the patient									Circadian component (%)*
	Age (years)	Biol. sex	Collection site	Metastatic	ALK status	TP53 status	PHOX2B status	ATRX status	MYCN status	
SKNSH	4	F	Bone marrow	yes	MUT	WT	MUT	WT	Normal	86.0
NGP	2.6	M	Lung	yes	WT	MUT	WT	WT	Amplified	71.6
GIMEN	3.5	F	Bone marrow	yes	WT	WT	WT	WT	Amplified	81.6
CLBGA	4	M	Bone marrow	yes	MUT	WT	WT	WT	Amplified	43.2
IMR5	1.1	M	Abdomen	yes	WT	WT	WT	WT	Amplified	24.0
LAN5	0.4	M	Bone marrow	yes	MUT	WT	WT	WT	Amplified	46.1
SKNAS	8	F	Bone marrow	yes	WT	MUT	WT	WT	Normal	27.6
KELLY	1	F	Autonomic ganglia	primary	MUT	MUT	WT	WT	Amplified	24.0
SKNBE(1)	1.7	M	Bone marrow	yes	WT	MUT	WT	MUT	Amplified	7.3
SKNBE(2)	2.2	M	Bone marrow	yes	WT	MUT	WT	MUT	Amplified	47.0
SH-SY5Y	4	F	Bone marrow	yes	MUT	WT	MUT	WT	Normal	17.6
CHP212	1.8	M	CNS	primary	WT	WT	WT	WT	Amplified	3.6

F, female; M, male; MUT, mutated; WT, wild-type; CNS, central nervous system. *Note: circadian component characterized by MRA in this study.

Table S3. Overview of drugs evaluated for neuroblastoma cell sensitivity and their disease relevance, Related to Figure 4.

Drug name	Target(s)	Target pathway(s)	Neuroblastoma (NB) relevance		Ref.
			NB model	Finding	
17-AAG (Tanespimycin)	HSP90	Protein stability and degradation	SKNSH cells; SKNSH xenograft	In vitro and in vivo growth inhibition, in vitro apoptosis-inducing and migration-inhibiting	3,4
AEW541	IGF-1R	Other, kinases	SKNAS, SKNBE(2), SH-SY5Y, LAN5, and IMR5 cells; SKNBE(2)-xenograft	Antiproliferative effect, sensitizing effect to cisplatin-induced apoptosis, in vivo tumor growth inhibition with little toxicity	5,6
AZD0530	ABL, SRC	Other, kinases	-	-	-
AZD6244	MEK	MAPK/ERK pathway	SKNSH, SKNAS, KELLY, NGP, and CHP212 cells	In vitro growth inhibition, particularly in CHP212 cells	7
Erlotinib (Tarceva)	EGFR	EGFR signaling	SKNSH, SH-SY5Y, NGP, and SKNAS cells; phase I clinical study	Limited anti-tumor responses in vitro, in vivo, and in patients.	8,9
L685458	γ-secretase	NOTCH signaling, UPP pathway	Diverse NB cells & patient-derived NB xenograft	in vitro and in vivo anti-tumor efficacy, no gastrointestinal toxicity in mice	10
Lapitinib (Tykerb)	EGFR, ERBB2	EGFR / RTK signaling	SH-SY5Y, SKNSH, SKNAS, and KELLY cells; transgenic zebrafish	synergistic anti-tumor effects YM155 [survivin-suppressor] in vitro and in vivo; synergistic anti-tumor effects with THZ1 [CDK7 inhibitor] in MYCN-amplified NB cells	11,12
LBW242	IAPs	Apoptotic pathway	KELLY, SKNAS, SKNBE(2), and SKNSH cells; NXS2 cell-based NB mouse	Sensitizing NB cells to chemotherapy-induced apoptosis; in vivo tumor growth inhibition; synergistic anti-proliferative effects with topoisomerase inhibitors in vitro	13,14
Nutlin3	p53-MDM2	p53 pathway	NGP, LAN5, SH-SY5Y, and GIMEN cells; chemo-resistant NB xenograft	In vitro growth inhibition and apoptosis induction in MYCN-amplified NB cells; in vivo tumor growth inhibition of chemo-resistant NB xenograft model.	15-17
Paclitaxel	Microtubules	Mitosis inhibitor	SKNSH and SH-SY5Y cells	Apoptosis-inducing	18,19

Panobinostat	HDAC	Chromatin histone acetylation	SKNSH, SKNBE(2), and SKNAS cells; TH-MYCN mouse	synergistic anti-tumor effects with other cytotoxic agents in vitro and in vivo	20,21
PD0325901	MEK1, MEK2	MAPK/ERK pathway	SKNAS, CHP212, and NGP cells	in vitro growth inhibition in NRAS mutant NB	22
PF2341066 (Crizotinib)	MET, ALK, ROS1	RTK signaling	Phase I clinical study.	Modest anti-tumor activity in NB patients.	23
PHA665752	MET	RTK signaling	SH-SY5Y, SHEP	in vitro growth inhibition in c-Met-positive NB cells	24
PLX4720	BRAF	RAS-RAF-MEK-ERK pathway	-	-	-
Sorafenib (Nexavar)	PDGFR, KIT, VEGFR, RAF	Other, kinases	SKNAS and other NB cell lines; NB xenograft; Phase I clinical study	In vitro and in vivo growth inhibition; limited reponse in clinical trials as combination therapy with topotecan.	25-27
TAE684	ALK	RTK signaling	LAN5, SH-SY5Y, SKNBE(2), and SKNAS; R1275Q xenograft	Antitumor activity in vitro and in vivo; inhibition of ALK phosphorylation in vivo.	28
TKI258 (Dovitinib)	RTK	Other, kinases	-	-	-
Topotecan	TOP1	DNA replication	Phase II clinical study	Part of combination therapy with temozolomide or cyclophosphamide	29,30
ZD6474 (Vandetanib)	EGFR, VEGFR, RET	EGFR / VEGFR signaling	SKNSH, SH-SY5Y, NGP, and SKNAS cells	In vitro and in vivo growth inhibition;	8

Frontline drugs:

- **Vincristine** – binds β-tubulin, preventing microtubule assembly and arresting mitosis.
- **Cisplatin** – creates intra- and inter-strand DNA cross-links that trigger apoptosis.
- **Cyclophosphamide** (**Frindovyx**) – alkylates and cross-links DNA, blocking replication.
- **Doxorubicin** – intercalates DNA and inhibits topoisomerase II, generating lethal strand breaks.
- **Dinutuximab / Unituxin** – monoclonal antibody directed at the GD2 disialoganglioside on neuroblastoma cells.
- **Naxitamab / Danyelza** – humanized anti-GD2 antibody (same GD2 target).
- **Iwilfin / Eflornithine** – irreversible inhibitor of ornithine decarboxylase (ODC), depleting polyamines.

References

1. Thiele, C.J. (1999). Neuroblastoma. In Human Cell Culture: Cancer Cell Lines Part 1, J.R.W. Masters, and B. Palsson, eds. (Springer Netherlands), pp. 21-53. 10.1007/0-306-46872-7_2.
2. Barretina, J., Caponigro, G., Stransky, N., Venkatesan, K., Margolin, A.A., Kim, S., Wilson, C.J., Lehár, J., Kryukov, G.V., Sonkin, D., et al. (2012). The Cancer Cell Line Encyclopedia enables predictive modelling of anticancer drug sensitivity. Nature *483*, 603-607. https://doi.org/10.1038/nature11003.
3. Hanna, R., Abdallah, J., and Abou-Antoun, T. (2021). A Novel Mechanism of 17-AAG Therapeutic Efficacy on HSP90 Inhibition in MYCN-Amplified Neuroblastoma Cells. Frontiers in Oncology *Volume 10 - 2020*. https://doi.org/10.3389/fonc.2020.624560.
4. Kang, J., Kamal, A., Burrows, F.J., Evers, B.M., and Chung, D.H. (2006). Inhibition of Neuroblastoma Xenograft Growth by Hsp90 Inhibitors. Anticancer Research *26*, 1903-1908.
5. Guerreiro, A.S., Boller, D., Shalaby, T., Grotzer, M.A., and Arcaro, A. (2006). Protein kinase B modulates the sensitivity of human neuroblastoma cells to insulin-like growth factor receptor inhibition. International Journal of Cancer *119*, 2527-2538. https://doi.org/10.1002/ijc.22126.
6. Tanno, B., Mancini, C., Vitali, R., Mancuso, M., McDowell, H.P., Dominici, C., and Raschellà, G. (2006). Down-Regulation of Insulin-Like Growth Factor I Receptor Activity by NVP-AEW541 Has an Antitumor Effect on Neuroblastoma Cells In vitro and In vivo. Clinical Cancer Research *12*, 6772-6780. https://doi.org/10.1158/1078-0432.Ccr-06-1479.
7. Dorel, M., Klinger, B., Mari, T., Toedling, J., Blanc, E., Messerschmidt, C., Nadler-Holly, M., Ziehm, M., Sieber, A., Hertwig, F., et al. (2021). Neuroblastoma signalling models unveil combination therapies targeting feedback-mediated resistance. PLOS Computational Biology *17*, e1009515. https://doi.org/10.1371/journal.pcbi.1009515.
8. Beaudry, P., Nilsson, M., Rioth, M., Prox, D., Poon, D., Xu, L., Zweidler-Mckay, P., Ryan, A., Folkman, J., Ryeom, S., and Heymach, J. (2008). Potent antitumor effects of ZD6474 on neuroblastoma via dual targeting of tumor cells and tumor endothelium. Molecular Cancer Therapeutics *7*, 418-424. https://doi.org/10.1158/1535-7163.Mct-07-0568.
9. Jakacki, R.I., Hamilton, M., Gilbertson, R.J., Blaney, S.M., Tersak, J., Krailo, M.D., Ingle, A.M., Voss, S.D., Dancey, J.E., and Adamson, P.C. (2008). Pediatric Phase I and Pharmacokinetic Study of Erlotinib Followed by the Combination of Erlotinib and Temozolomide: A Children's Oncology Group Phase I Consortium Study. Journal of Clinical Oncology *26*, 4921-4927. https://doi.org/10.1200/jco.2007.15.2306.
10. Dorneburg, C., Goß, A.V., Fischer, M., Roels, F., Barth, T.F., Berthold, F., Kappler, R., Oswald, F., Siveke, J.T., Molenaar, J.J., et al. (2016). γ-Secretase inhibitor I inhibits neuroblastoma cells, with NOTCH and the proteasome among its targets. Oncotarget *7*, 62799-62813. https://doi.org/10.18632/oncotarget.11715.
11. Radic-Sarikas, B., Halasz, M., Huber, K.V.M., Winter, G.E., Tsafou, K.P., Papamarkou, T., Brunak, S., Kolch, W., and Superti-Furga, G. (2017). Lapatinib potentiates cytotoxicity of YM155 in neuroblastoma via inhibition of the ABCB1 efflux transporter. Scientific Reports *7*, 3091. https://doi.org/10.1038/s41598-017-03129-6.

12. Tee, A.E., Ciampa, O.C., Wong, M., Fletcher, J.I., Kamili, A., Chen, J., Ho, N., Sun, Y., Carter, D.R., Cheung, B.B., et al. (2020). Combination therapy with the CDK7 inhibitor and the tyrosine kinase inhibitor exerts synergistic anticancer effects against MYCN-amplified neuroblastoma. International Journal of Cancer *147*, 1928-1938. https://doi.org/https://doi.org/10.1002/ijc.32936.
13. Eschenburg, G., Eggert, A., Schramm, A., Lode, H.N., and Hundsdoerfer, P. (2012). Smac Mimetic LBW242 Sensitizes XIAP-Overexpressing Neuroblastoma Cells for TNF-α–Independent Apoptosis. Cancer Research *72*, 2645-2656. https://doi.org/10.1158/0008-5472.Can-11-4072.
14. Najem, S., Langemann, D., Appl, B., Trochimiuk, M., Hundsdoerfer, P., Reinshagen, K., and Eschenburg, G. (2016). Smac mimetic LCL161 supports neuroblastoma chemotherapy in a drug class-dependent manner and synergistically interacts with ALK inhibitor TAE684 in cells with ALK mutation F1174L. Oncotarget *7*, 72634-72653. https://doi.org/10.18632/oncotarget.12055.
15. Gamble, L.D., Kees, U.R., Tweddle, D.A., and Lunec, J. (2012). MYCN sensitizes neuroblastoma to the MDM2-p53 antagonists Nutlin-3 and MI-63. Oncogene *31*, 752-763. https://doi.org/10.1038/onc.2011.270.
16. Van Maerken, T., Ferdinande, L., Taildeman, J., Lambertz, I., Yigit, N., Vercruysse, L., Rihani, A., Michaelis, M., Cinatl, J., Jr., Cuvelier, C.A., et al. (2009). Antitumor activity of the selective MDM2 antagonist nutlin-3 against chemoresistant neuroblastoma with wild-type p53. J Natl Cancer Inst *101*, 1562-1574. https://doi.org/10.1093/jnci/djp355.
17. Van Maerken, T., Rihani, A., Dreidax, D., De Clercq, S., Yigit, N., Marine, J.-C., Westermann, F., De Paepe, A., Vandesompele, J., and Speleman, F. (2011). Functional Analysis of the p53 Pathway in Neuroblastoma Cells Using the Small-Molecule MDM2 Antagonist Nutlin-3. Molecular Cancer Therapeutics *10*, 983-993. https://doi.org/10.1158/1535-7163.Mct-10-1090.
18. André, N., Carré, M., Brasseur, G., Pourroy, B., Kovacic, H., Briand, C., and Braguer, D. (2002). Paclitaxel targets mitochondria upstream of caspase activation in intact human neuroblastoma cells. FEBS Letters *532*, 256-260. https://doi.org/10.1016/S0014-5793(02)03691-8.
19. Riccardi, A., Servidei, T., Tornesello, A., Puggioni, P., Mastrangelo, S., Rumi, C., and Riccardi, R. (1995). Cytotoxicity of paclitaxel and docetaxel in human neuroblastoma cell lines. Eur J Cancer *31a*, 494-499. https://doi.org/10.1016/0959-8049(95)00056-o.
20. Irwin, M.S., Naranjo, A., Zhang, F.F., Cohn, S.L., London, W.B., Gastier-Foster, J.M., Ramirez, N.C., Pfau, R., Reshmi, S., Wagner, E., et al. (2021). Revised Neuroblastoma Risk Classification System: A Report From the Children's Oncology Group. J Clin Oncol *39*, 3229-3241. https://doi.org/10.1200/jco.21.00278.
21. Waldeck, K., Cullinane, C., Ardley, K., Shortt, J., Martin, B., Tothill, R.W., Li, J., Johnstone, R.W., McArthur, G.A., Hicks, R.J., and Wood, P.J. (2016). Long term, continuous exposure to panobinostat induces terminal differentiation and long term survival in the TH-MYCN neuroblastoma mouse model. International Journal of Cancer *139*, 194-204. https://doi.org/10.1002/ijc.30056.
22. Kiessling, M.K., Curioni-Fontecedro, A., Samaras, P., Lang, S., Scharl, M., Aguzzi, A., Oldrige, D.A., Maris, J.M., and Rogler, G. (2016). Targeting the mTOR Complex by Everolimus in NRAS Mutant Neuroblastoma. PLoS One *11*, e0147682. https://doi.org/10.1371/journal.pone.0147682.

23. Mossé, Y.P., Lim, M.S., Voss, S.D., Wilner, K., Ruffner, K., Laliberte, J., Rolland, D., Balis, F.M., Maris, J.M., Weigel, B.J., et al. (2013). Safety and activity of crizotinib for paediatric patients with refractory solid tumours or anaplastic large-cell lymphoma: a Children's Oncology Group phase 1 consortium study. Lancet Oncol *14*, 472-480. https://doi.org/10.1016/s1470-2045(13)70095-0.
24. Crosswell, H.E., Dasgupta, A., Alvarado, C.S., Watt, T., Christensen, J.G., De, P., Durden, D.L., and Findley, H.W. (2009). PHA665752, a small-molecule inhibitor of c-Met, inhibits hepatocyte growth factor-stimulated migration and proliferation of c-Met-positive neuroblastoma cells. BMC Cancer *9*, 411. https://doi.org/10.1186/1471-2407-9-411.
25. Kakodkar, N.C., Peddinti, R.R., Tian, Y., Guerrero, L.J., Chlenski, A., Yang, Q., Salwen, H.R., Maitland, M.L., and Cohn, S.L. (2012). Sorafenib inhibits neuroblastoma cell proliferation and signaling, blocks angiogenesis, and impairs tumor growth. Pediatric Blood & Cancer *59*, 642-647. https://doi.org/10.1002/pbc.24004.
26. Reed, D.R., Mascarenhas, L., Manning, K., Hale, G.A., Goldberg, J., Gill, J., Sandler, E., Isakoff, M.S., Smith, T., Caracciolo, J., et al. (2016). Pediatric phase I trial of oral sorafenib and topotecan in refractory or recurrent pediatric solid malignancies. Cancer Medicine *5*, 294-303. https://doi.org/10.1002/cam4.598.
27. Okada, K., Nakano, Y., Yamasaki, K., Nitani, C., Fujisaki, H., and Hara, J. (2016). Sorafenib treatment in children with relapsed and refractory neuroblastoma: an experience of four cases. Cancer Medicine *5*, 1947-1949. https://doi.org/10.1002/cam4.784.
28. Regairaz, M., Munier, F., Sartelet, H., Castaing, M., Marty, V., Renauleaud, C., Doux, C., Delbé, J., Courty, J., Fabre, M., et al. (2016). Mutation-Independent Activation of the Anaplastic Lymphoma Kinase in Neuroblastoma. The American Journal of Pathology *186*, 435-445. https://doi.org/10.1016/j.ajpath.2015.10.016.
29. Ashraf, K., Shaikh, F., Gibson, P., Baruchel, S., and Irwin, M.S. (2013). Treatment with topotecan plus cyclophosphamide in children with first relapse of neuroblastoma. Pediatr Blood Cancer *60*, 1636-1641. https://doi.org/10.1002/pbc.24587.
30. Di Giannatale, A., Dias-Gastellier, N., Devos, A., Mc Hugh, K., Boubaker, A., Courbon, F., Verschuur, A., Ducassoul, S., Malekzadeh, K., Casanova, M., et al. (2014). Phase II study of temozolomide in combination with topotecan (TOTEM) in relapsed or refractory neuroblastoma: a European Innovative Therapies for Children with Cancer-SIOP-European Neuroblastoma study. Eur J Cancer *50*, 170-177. https://doi.org/10.1016/j.ejca.2013.08.012.